De novo organelle biogenesis in the cyanobacterium TDX16 released from the green alga *Haematococcus pluvialis*

Qing-lin Dong*, Xiang-ying Xing, Yang Han, Xiao-lin Wei, Shuo, Zhang

Department of Bioengineering, Hebei University of Technology, Tianjin 300130, China

*Correspondence: qldong@hebut.edu.cn

Abstract

It is generally accepted that eukaryotic cell arises from prokaryotic cell, which means that organelle can be formed in prokaryotic cell. However, no such an instance has been detected till now. Here, we report organelle biogenesis in the endosymbiotic cyanobacterium TDX16 released from the green alga *Haematococcus pluvialis*, which occurred through six steps. (1) An inner intracytoplasmic membrane (IIM), an outer intracytoplasmic membrane (OIM) and an intervening peptidoglycan-like layer (PL) were synthesized by merging cytoplasmic membrane (CM)-derived thick margin vesicles, which partitioned the thylakoid-less cytoplasm into three compartments: an inner cytoplasm (ICP), an outer cytoplasm (OCP) and a sandwiched intracytoplasmic space (IS). (2) Osmiophilic granules that blistered from CM, OIM and IIM developed into primary thylakoids (PT) in ICP; while OCP disappeared and thus OIM and CM combined into a double-membraned cytoplasmic envelope (CE). (3) ICP decondensed; IIM and PT disassembled into tiny vesicles (TV) and double-membraned vesicles (DMV) respectively. Such that DNA fibers (DF) aggregated and migrated to PL. (4) TV fused into a double-membraned intracytoplasmic envelope (ICE), which re-compartmentalized the coalesced IS and ICP into a new intracytoplasmic space (NS) sequestering most DF and a new inner cytoplasm (NIC) with only few DF. Then ribosomes were formed in both NS and NIC, while DMV opened and extended into secondary thylakoids (ST) only in NIC. (5) NIC developed into the primitive chloroplast (PC) surrounded by ICE, in which ST disassembled, while ST-derived plastoglobuli developed into primitive eukaryotic thylakoids (PMT). After PL dismantled, the matrix of NS was concentrated and encased with the membranes synthesized from ICE-derived dotted vesicles into the primitive nucleus (PN). So, NS vanished, CE wrapped PC and PN. Outside CE, eukaryotic cell wall was formed by assembling sheath at the outer membrane of original cell wall and modifying the peptidoglycan layer. (6) Eukaryotic cytoplasm was built up from the matrix extruded from PN. Mitochondria were assembled in and segregated from PC by encapsulating a portion of stroma with the membranes synthesized from PMT-derived dense-margined vesicles. Then, most mitochondria turned into double-membraned vacuoles after matrix degradation, which mediated unconventional exocytosis and endocytosis. When this process finished, PN got matured into a nucleus enclosed by two sets of envelopes; PC matured into a chloroplast with its PMT maturing into thylakoids. Consequently, the prokaryotic TDX16 cell developed into a eukaryotic cell (TDX16-DE). Results of pigment analyses and 16S rRNA sequencing revealed that TDX16-DE chloroplast contained chlorophyll b and lutein showing 99% similarity to that of *Chlorella vulgaris*, TDX16 was a phycocyanin-containing cyanobacterium resembling *Chroococcidiopsis thermalis* (98% identity). Whereas, TDX16's genome size (15,333,193 bp) and gene number (13,415) were 2.43 and 2.40 times those of *C. thermalis* (6,315,792 bp; 5593 genes) respectively, indicating that TDX16 acquired at least 7822 genes from its host *H. pluvialis*. Therefore, the mechanism underlying organelle biogenesis in TDX16 was the integration and expression of the obtained genes.

Key words: De novo organelle biogenesis; endosymbiotic cyanobacterium; *Haematococcus pluvialis*

1. Introduction

All cells are structurally categorized into two groups: eukaryotic cell and prokaryotic cell. Eukaryotic cell contains membrane-bounded compartments called organelles, in which distinct reactions take place. So, organelle biogenesis is essential for cell maintenance and proliferation, which was thought to be achieved only by fission of the preexisting one. Nonetheless, recent studies demonstrated that organelles in the secretory pathway can be formed de novo, including Golgi apparatus (Rossanese et al., 1999; Bevis et al., 2002; Glick 2002; Tängemo et al. 2010; Abiodun and Matsuoka 2013), peroxisomes (South and Gould 1999; Hoepfner et al., 2005; Kim et al., 2006; Ruckt äschel et al., 2007; Motley and Hettema 2007; Huber et al., 2012; Opalińsk et al., 2012; van der Zand et al., 2012; Sugiura et al., 2017; Hettema and Gould 2017); lysosomes (Kornfeld and Mellman 1989; Blott and Griffiths 2002; Liu et al., 2005; Saftig and Klumperman 2009; Luzio et al., 2014; Li et al., 2016; Perera and Zoncu 2016) and vacuoles (Berjak 1972; Marty 1978; Herman et al., 1994; Hoh et al., 1995; Olbrich et al., 2007; Viotti et al., 2013). These results imply that, provided with the information encoded in the genetic material and the machinery needed to interpret this, the cell can produce the organelle with no information in the form of a template or copy of the organelle (Lowe and Barr 2007).

In sharp contrast to eukaryotic cell, prokaryotic cell has no organelle. It is widely accepted that eukaryotic cell originates from prokaryotic cell, which means that organelle can be formed in the latter. Paradoxically, however, no instance of organelle biogenesis in prokaryotic cell had been detected. In this case, it was assumed that organelle biogenesis in prokaryotic cell occurred only once, during which the first nucleus was formed in an ancient prokaryotic cell, giving rise to the ancestor of eukaryotic cell. Nevertheless, there is another possibility: organelle biogenesis in prokaryotic cell occurred quickly in a short time resulting in the sudden transition of a prokaryotic cell into a eukaryotic cell, and thus was hard to capture.

In the previous study we found unexpectedly that the necrotic cells of unicellular green alga *Haematococcus pluvialis* burst and liberated countless small blue cyanobacterial cells (TDX16) in the adverse conditions of high temperature and low irradiance (Dong et al., 2011). TDX16 was light-sensitive, which was relatively stable in the dim light, but turned readily into small green *Chlorella*-like algal cell as light intensity elevated (Dong et al., 2011). The time required for TDX16's transition was short and negatively related to the light intensity, which was about 10 days at 60 μmol photons m^{-2} s^{-1}. However, light above 60 μmol photons m^{-2} s^{-1} was lethal, causing the disruption of TDX16 cell.

TDX16's incredible change was puzzling, which prompted us to investigate if, how and why organelles were formed in its prokaryotic cell. The present study unveiled the biogenesis of

chloroplast, nucleus, mitochondrion and vacuole as well as other eukaryotic structures within the thylakoid-less TDX16 cell, owing to the integration and expression of the acquired genes.

2. Results

2.1 Unusual structure and variable nature of TDX16

Under low light condition, TDX16 cells were always surrounded by thick sheaths (extracellular matrix) and further enclosed within the sporangia (Fig.1-2), showing some similarities to the endospores (baeocytes) of *Chroococcidiopsis* (Waterbury and Stanier, 1978; Büdel and Rhiel 1985; Caiola et al., 1993; Caiola et al., 1996; Billi et al., 2000). Most unusually, cells in the same or different sporangia remained at different developmental states with some different inclusions (Fig.1-2). As shown in Fig.1, three different-sized cells (endospores) in a multilayered sporangium were all devoid of thylakoid, but contained one or two membrane-limited heterogenous globular bodies (HGB), and a varied number of cyanobacterial inclusions, including carboxysomes (polyhedral bodies, CX) (Shively et al., 1973; Yeates et al., 2008), polyphosphate bodies (PB) (Allen 1984), osmiophilic granules (lipid globules/bodies, OG) (Lang 1968). HGB contained DNA-like electron-dense granules and filaments and always situated in the nucleoids (NU), where DNA fibers (DF) (Robinow and Kellenberger 1994; Eltsov and Zuber 2006) and ribosomes (RB) (Meene et al., 2006) scattered. The important difference among these cells was that some small swirly and rod-shaped electron-transparent vesicles (EV) were being developed in the left large cell. Similarly, in another five-cells-containing sporangium (Fig.2), the bottom cell contained only OG, while many large different-shaped EV were being formed in the three middle cells, and several thylakoid-like structures were built up in the upper cell.

It was evident that EV developed from OG, because (1) OG presented in the small EV, some of them were, however, not in the section plane and thus invisible; (2) as EV enlarged, OG turned into ring-shaped vesicles (RV) after their dense matrixes degraded into to opaque and finally transparent materials (Fig.1-2). OG contained triacylglycerol and tocopherol (Peramuna and Summers 2014), while its exact composition and structure was as yet unknown. There was a general consensus that OG in cyanobacterial cell was comparable to plastoglobuli (PG) in algal and plant chloroplasts (Lang, 1968; Brown and Bisalputra 1969; Findley, 1970; Bréhélin et al., 2007), which contained lipids, enzymes, proteins e.g., IM30/ Vipp1 protein (vesicle-inducing protein in plastids 1) and carotenoids, and structurally consisted of a monolayer lipid membrane (half-unit membrane) and a neutral lipid core (Hansmann and Sitte 1982; Smith et al. 2000; Austin et al., 2006; Ytterberg et al., 2006; Vidi etal., 2006; Bréhélin and Kessler 2008; Lichtenthaler 2013; Davidi et al., 2015). Nevertheless, the formation of RV in EV indicated that OG had two

monolayer lipid membranes, which most likely encased a hydrophilic “protein core”, while the intermembrane space was filled with neutral lipids. So, as the intermembrane space dilated owing to the synthesis of low-density lipids or the like, the outer monolayer membrane bulged and gave rise to an EV; while the interior monolayer membrane and the protein core remained as a monolayer membrane-bounded OG, which subsequently transformed into a RV after the protein core was metabolized or degraded for membrane-remodeling (Fig.1-2).

The above results demonstrated that unlike the genuine thylakoid-less cyanobacterium *Gloeobacter violaceus* (Rippka et al., 1974), TDX16 was hypersensitive to light and highly variable in nature, whose anomalous change could not be inhibited completely even in the dim light. Therefore, it was not surprising that when grew in high light regime, TDX16 changed fundamentally in cell structure and pigmentation which were described in the following sections.

2.2 Compartmentalization and biogenesis of primary thylakoids

2.2.1 Synthesis of intracytoplasmic membranes and peptidoglycan-like layer

Under high light intensity, TDX16 with surrounded sheath escaped from the ruptured sporangium and changed rapidly in structures and inclusions (Fig.3A). PB and CX disappeared, HGB became nearly empty leaving only few DNA-like fibrils and electron-dense margin residues; while a startling number of OG and stacks of membranous elements emerged, and many small EV were being developed (Fig.3A).

The most striking change was, however, the compartmentalization of cytoplasm that was enclosed by the cytoplasmic membrane (CM) (Fig.3A). TDX16’s cell wall, like those of other cyanobacteria and gram-negative bacteria (Edwards, et al., 1968; Glauert and Thornley 1969; Hobot, 1984; Beveridge, 1999; Hoiczyk and Hansel 2000; Liberton et al., 2006), comprised an outer membrane (OM) and an electron-dense peptidoglycan layer (P), which was separated from CM by an electron-transparent extracytoplasmic (periplasmic) space (ES) (Fig.3A). Inside the cytoplasm, two intracytoplasmic membranes and an intervening peptidoglycan-like layer (PL) were being synthesized, which initiated from a start point and extended parallel to CM (Fig.3A). As a result, the cytoplasm was partitioned into three compartments: (1) the inner cytoplasm (ICP) delimited by the inner intracytoplasmic membrane (IIM), (2) the outer cytoplasm (OCP) of variable thickness bounded by the outer intracytoplasmic membrane (OIM) and CM, and (3) a sandwiched intracytoplasmic space (IS) that was further separated by PL into an outer intracytoplasmic space (OIS) and an inner intracytoplasmic space (IIS) (Fig.3A). It was important that OCP began to reduce or degrade in localized regions near the start point, such that OIM got

closed to but not connected with CM (Fig.3A). Compartmentalization also commenced in some cells growing in the low light just as the formation of EV (Fig.1-2). In all these cases, there was no continuity between the intracytoplasmic membranes and CM, and thus the formers were not developed by invagination of the latter. Instead, OIM, IIM and PL were synthesized synchronously by fusion of the small thick margin vesicles (TMV) blistered form the inner leaflet of CM (Fig.3A), which occurred in two probable ways: (1) if TMV were delimited by a half-unit membrane, they first released their contents for synthesizing the septal PL and then fused alternately on its two sides; (2) if TMV were limited by a unit membrane, as they fused one another, the septal PL was synthesized within the coalesced vesicles, a scenario somewhat similar to the formation of cell plate during cytokinesis (Samuels et al., 1995).

2.2.2 Production of OG

Concurrent with compartmentalization, plentiful OG of various sizes blistered from the inner and outer leaflets CM (Fig.3A), such a scenario was also observed in the cells growing under low light condition but the numbers of OG were limited (Fig.1-2). More importantly, some small OG also budded from the inner leaflet of OIM and outer leaflet of IIM (Fig. 3A). These results suggested that the newly formed OIM and IIM were comparable or equivalent to the multifunctional CM, on which both photosynthesis and respiration performed just like the case of the cytoplasmic membrane of *Gloeobacter violaceus* (Rippka et al., 1974; Rexroth et al., 2001), and many metabolites were synthesized as were the cases in the cytoplasmic membranes of all cyanobacteria. These metabolites included (1) peptidoglycan (Egan et al., 2016), phospholipid and lipid intermediates (Osborn et al., 1972); (2) chlorophyll precursors (Peschek et al., 1989) and carotenoid (Bullerjahn and Sherman, 1986); (3) photosystem core complexes (Smith and Howe 1993; Zak et al., 2001; Keren et al., 2005) and (4) IM30/ Vipp1 protein (Li et al., 1994; Westphal et al., 2001; Huang et al., 2002; Srivastava et al., 2006) that was proposed to be involved in genesis of thylakoid membranes (Li et al., 1994; Westphal et al., 2001; Aseeva et al., 2007), or assembly of photosystems (Gao and Xu 2009; Zhang et al., 2014).

OG was formed by protrusion of the bilayer of CM, OIM and IIM as they were enclosed by two half-unit membranes (Fig.1-2) and apparently played different roles. OG blistered from the inner leaflet of CM, OIM and IIM migrated into ICP for development of EV (Fig.3A); while those shed from the outer leaflet of CM contacted CW, and thus severed as transport conduits or trafficking vehicles channeling or transferring lipids and carotenoids from CM to the CW (Fig.3A), because these compounds were the constituents of OM (Resch and Gibson, 1983; Jürgens and Weckesser 1985; Hoiczyk and Hansel 2000).

2.2.3 Formation of EV and double-membraned cytoplasmic envelope

As OIM, IIM and PL extended (Fig.3B) and ultimately closed up (Fig.3C), the small EV elongated (Fig.3B) and dilated asymmetrically into swirling ones spiraling around NU, and OG began to merge into large ones (Fig.3C). Thereafter HGB disappeared, while new EV were developed within NU and several electron-opaque particles (EOP) were formed (Fig. 3D). In parallel with these changes, the narrow IS (Fig. 3BC) became widened filling with electron-opaque materials (EOM) (Fig. 3D), while OCP disappeared, such that OIM and CM combined into a double-membraned cytoplasmic envelope (CE) (Fig. 3D), which abutted CW owing to the narrowing of ES (Fig.3D). During this process a mass of electron-dense materials were synthesized on CE and transferred to CW for assembling SH, and thus made these structures indistinct (Fig.3D). SH was loosely compacted, made up of flocculent fibrillary materials (FM), microvesicles (MV) and electron-translucent vesicles (ELV) (Fig.3D).

2.2.4 Development of EV into primary thylakoids

The intraluminal RV swelled up into a dilated-ring-shaped vesicle (DRV), whose membrane ultimately met and combined with EV membrane, giving rise to a unit-membrane-bounded combined vesicle (CV); and then CV coalesced into long ones or flattened out into short slender sacs, termed primary thylakoid (PT) (Fig.4A). In this way, EV developed progressively into short PT with opaque matrix, distributing randomly in ICP (Fig.4B). The short PT further extended or merged end-to-end into long PT; while the long coalesced CV flattened out into PT by localized-constriction. And concurrently several cyanophycin granules (CG) (Lang and Fisher 1969; Simon 1973) and EOP were formed (Fig. 4C). Finally, the long PT were adjusted to be parallel-arranged, on which the extrinsic phycobilisomes (PCB) (Gantt and Conti 1969) were assembled (Fig.4D). Compared to other cyanobacterial thylakoids, PT exhibited primordial features: thick margin, wide luminal space and spacing (interthylakoidal distances).

Accompanying PT biogenesis, a number of ELV shed from OM into SH (Fig.4A), and a mass of DNA fibers were synthesized in ICP (Fig.4D). Occasionally, a group of small RV presented in an EV (Fig.4B), which was probably formed during OG fusion (Fig. 4A) and merged later into large one.

2.3 Re-compartmentalization, DNA translocation and repartition, and biogenesis of secondary thylakoids

2.3.1 Disassembly of PT and IIM, decondensation of ICP and DNA translocation

The newly formed PT promoted TDX16's photosynthetic capacity, but were disassembled soon afterwards. As shown in Fig.5A, PT disassembly initiated with the condensation of luminal matrix, such that PT membrane pair was in closely apposition, seeming to be a single membrane with rough margin. In the meantime, ICP decondensed (solubilized) and became translucent, in which short DF dispersed, some less electron-dense materials (LDM), less electron-dense bodies (LDB) and CG were formed (Fig.5A); IIM disassembled into tiny vesicles (TV), so LDM diffused outward, blurring the compacted PL, CE and CW (Fig. 5A). Subsequently, the solubilized ICP was separated into two portions by LDM: in the lower portion, PT broke up into double-layered membrane fragments (DMF, two unit membranes) and in parallel DF aggregated; while in the upper portion, DMF began to curl and merge laterally into double-membraned vesicles (DMV) (Fig.5B). When all DMF disappeared, a crowd of DMV was formed and numerous DF aggregated (Fig.5C). Thereafter, DMV moved outward quickly and attached to PL that was cover by electron-dense materials, while the intermingled DF scattered outward slowly resulting in an "empty" inner space (EIS), at the border of which the recruited TV began to fuse into double-layered membrane segments (DMS) (Fig. 5D).

2.3.2 Re-compartmentalization, DNA reallocation and formation of secondary thylakoids

As DMS coalesced and extended into a double-membraned intracytoplasmic envelope (ICE), the coalesced ICP and IIS was re-compartmentalized into a new inner cytoplasm (NIC) and a new inner intracytoplasmic space (NIS) (Fig.6A). NIC was enclosed by ICE; while NIS represented the space between ICE and PL. Most DF was allocated into NIS, which decondensed into cloudlike materials or aggregated into thick threads; by contrast only few sporadic DF and electron-dense particles (EP) were portioned into NIC (Fig.6A). ICE was not sealed, on the outer leaflet of which, some electron-transparent materials were synthesized (Fig.6A), similar in appearance to the bacterial lipid (Packter and Olukoshi 1995; Alvarez et al., 1996; Kalscheuer et al., 2007). Accompanying ICE expansion, DF in the narrowing NIS decondensed and attached to the thickened PL (Fig.6B); while DMV that were covered by LDM detached from PL, moving inward via ICE opening into NIC or outward through PL pores into OIS (Fig.6B). Therefore, the fenestrated PL served not only as a mechanical and osmotic barrier, but also a platform for anchoring DNA and DMV.

When ICE was sealed, DNA in NIS recondensed into thick DF with concomitant formation

of countless RB (Fig. 6C). Meanwhile, an increased number of DF and a myriad of RB were also formed in NIC; DMV opened up, retransformed into DMF (Fig. 6C). Thereafter, DMF extended randomly into spiral thylakoids, which was devoid of PCB and morphologically different from PT, termed secondary thylakoids (ST) (Fig.6D). Concomitant with the appearance of ST was the formation of OG and EOB as well as enrichment of DF and RB (Fig.6D). The structures outside of NIC were fuzzy owing to the diffusion of electron-dense materials: the major portion of PL dismantled, such that NIS and OIS coalesced into a new intracytoplasmic space (NS), whose content became the new intracytoplasmic matrix (NX). Aside from DMV, several large electron-translucent oblong vesicles (OV) and electron-opaque vesicles (EOV) emerged in NS (Fig.6D).

The viability of the cell indicated that NIC was capable of both photosynthesis and respiration just like a cyanobacterium. So, ST was equipped with photosynthetic and respiratory electron transfer chains as are the cyanobacterial thylakoids (Smith and Howe 1993; Cooley and Vermaas 2001; Lea-Smith et al., 2013; Mullineaux 2014). Whereas, NIC contained only a small amount of DNA, consequentially most of the proteins it required were synthesized in and imported from NX. Thus, NIC played the roles of chloroplast and mitochondrion, while NX served dual functions of nucleus and cytoplasm.

2.4 Biogenesis of primitive chloroplast, eukaryotic cell wall and primitive nucleus

2.4.1 Biogenesis of primitive eukaryotic thylakoids, primitive chloroplast and eukaryotic cell wall

Immediately after the emergence of transitional ST, drastic changes occurred in different compartments. As shown in Fig.7A, NIC became polarized, in which ST underwent disassembly, leaving some remnants in the lower region; while parallel arrays of discrete slender sacs with transparent matrix were being developed in the upper region (Fig.7A). These parallel-arranged slender sacs were morphologically similar to algal and plant thylakoids, termed the primitive eukaryotic thylakoids (PMT). Beneath PMT, a nascent pyrenoid (PD) with an incomplete starch plate (SP) and two starch granules (SG) were formed (Fig.7A), both of which were the characteristic bodies of green algal chloroplasts (Gibbs, 1962). So, NIC developed into a primitive chloroplast (PC) delimited by ICE. That was to say, ICE became the chloroplast envelope (CHE). PMT were developed from PG produced during disassembly of ST (Fig.7A), in a way similar but

not identical to the biogenesis of PT from OG (Fig.4). The absence of mitochondrion implied that respiration still performed on PMT. Thus, PC was a compound organelle sharing the functions of chloroplast and mitochondrion.

NS became widened and clear: NX condensed, containing RB and newly assembled chromatin fibers (CF) (Hay and Revel, 1963; Horowitz et al., 1994); PL and DMV disappeared, while many small dotted vesicles (DV) blistered from CHE and lined up along CE, some of which began to fuse and flattened into membrane segments (MS) (Fig.7A). Such a scenario of membrane synthesis was akin to the assembly of nuclear envelope in vitro or in vivo during open mitosis (Lohka and Masui 1983; Newport, 1987; Vigers and Lohka 1991; Jian et al., 1994). Furthermore, a large coated-vesicle-like opaque-periphery vesicle (OPV) was being assembled at CHE, which appeared to bridge CHE and CE for transferring substances.

The fluffy SH (Fig.6D) was organized into a multilayered one, which adhered to OM and made the latter hard to discern (Fig.7A). Such that the new stratified SH and CW seemed to be a continuum (entity), similar in appearance to the cell wall of eukaryotic cell, referred to as the eukaryotic cell wall (EW). The formation of new SH implied that CE and OM were remodeled, while the peptidoglycan layer (P) underlying OM turned into an electron-dense layer (EL). There were a large number of rounded or flattened small vesicles (SV) in the new SH, similar to the vesicles or 'fleck-like' membrane elements in the algal cell wall (Barton 1965; Meindl et al., 1992). Since some smaller vesicles (SMV) budded from the outer leaflet of CE (Fig.7A), it was conceivable that CE incorporated DMV or the like within NS (Fig.6D) for membrane expansion and then gave rise to SMV; in turn SMV were fused into OM, from which SV shed into the new SH.

2.4.2 Encapsulation of the concentrated NX into a primitive nucleus

As PG developed progressively into CV and then flattened into PMT with wide luminal space in the lower PC region, PD got matured, surrounded with a complete SP and bisected by two pairs of PMT. Hence, PC expanded substantially, occupying most NS (Fig.7B). Subsequently, PMT coalesced and extended around PD (Fig.7C). The membranes of adjacent PMT were connected, giving the appearance to be a single membrane. So, PC expanded further and occupied whole NS in the longitudinally sectioned planes; CHE adhered to CE, from the latter of which a dense vesicle (DSV) shed off into the widened ES (Fig.7C).Vertical profile (Fig.7D) showed that the anterior portion of NS disappeared owing to PC expansion, such that NX in the shrunken NS around the posterior portion of PC was concentrated by squeezing out liquid into ES, at the border of which MS coalesced into a limiting membrane (LM) (Fig.7D). As PC expansion continued, NX moved to (Fig. 7E) and finally converged at one side of PC, which was ensheathed by LM and

turned into the primitive nucleus (PN) (Fig. 7F). Consequently, LM became PN envelope (PNE), NS vanished, and in turn CE shrank and wrapped PC and PN (Fig. 7F).

PN sequestered the concentrated NX containing CF and RB (Fig. 7F) and thus, like PC, was also a compound organelle functioning as nucleus and eukaryotic cytoplasm; while PNE seemed to be consisted of four unit membranes, because it was synthesized by coalescence of DV, which budded from CHE and appeared being bounded by two unite membranes (Fig. 7A). Moreover, EW was osmotic-sensitive, whose outer layer SH shed frequently during cell fixation (Fig. 7 EF). This result confirmed that EW was loosely compacted owing, at least partially, to the insertion of SV and ELV.

2.5 Formation of eukaryotic cytoplasm and biogenesis of mitochondrion

2.5.1 Concurrent formation of eukaryotic cytoplasm and biogenesis of mitochondria

As shown in Fig.8A, a vesicle-containing body (VB), apparently derived from the invaginated PC, was being engulfed by PN with concomitant formation of a thin layer of electron-dense materials. PNE was contiguous with CE at the outer side, but separated into two sets of double membraned envelopes inside PC cavity, the inner and outer sets of which were referred to as nuclear envelope (NE) and outer nuclear envelope (OE) respectively. This result confirmed that PNE was consisted of four unit membranes. The thin layer of electron-dense materials was extruded from PN at the site where NE and OE fused, which contained RB and thus was the nascent eukaryotic cytoplasm (EM). Concurrent with the formation of EM, a small mitochondrion (M) was being assembled in PC. After ‘digestion’ of VB, PN and EM both increased in sizes; and an oval mitochondrion with characteristic cristae (CR) emerged in the apical dome of the enlarged PC cavity (Fig.8B). NE and OE were separated by an interenvelope space (IES), but merged at one site resulting in a wide opening, from which nuclear matrix (i.e. EM) was extruded. RB in EM were larger than those within the PC stroma (SM), most of which were attached to the organelles (Fig.8B). During this process, a number of SMV and microfibrils (ML) budded and emanated from CE into ES (Fig.8B). Concurrent nuclear matrix extrusion and mitochondrion formation were observed in different cells (Fig. 8CDE), and two spindle-shaped mitochondria were just being assembled in a PC (Fig. 8D). Occasionally, an intranuclear body (IB) appeared in a PN (Fig.8F), which seemed to be developed during engulfment and digestion of VB or the like, and play a role in selective extrusion of nuclear matrix.

2.5.2 Continuous biogenesis of mitochondria after building up EM

After formation of EM, bulk matrix extrusion from PN ceased, so PN got matured into nucleus (NU); while PC was not the case, in which new mitochondria were developed continuously even after the emergence of vacuoles (V) with internal vesicle (IV), multilamellar body (MLB), lipid droplet (LD), and small opaque vesicle (SOV), leading to the distortion of PMT (Fig.9). As shown in Fig.9A, a small mitochondrion was being developed at the PC edge; while a twisting dumbbell-shaped mitochondrion was nearly finished, one of its bulbous-end sequestering an internal body (ITB) was segregated, but another end was contiguous with PC (Fig.9B). Details of mitochondrion biogenesis were displayed during the assembly of giant mitochondria. As shown in Fig. 9C, a large unfinished 'L-shaped' mitochondrion was continuous with PC in the region around its corner point: the inner side envelope of its long arm and the corresponding portion of CHE, as well as the interior CR were nearly complete; while those of its short arm were just being synthesized. All these membranes were synthesized by merging the small dense-margined vesicles (DGV) developed from the segmented PMT (Fig.9C). Consequentially, mitochondria envelope (ME) and the corresponding portion of CHE were consisted of two unit-membranes; while CR, like PT, ST and PMT, was delimited by a unit-membrane. Similarly, in another cell a bulky mitochondrion was undergoing segregation, which was connected with PC on the inner side but a small mitochondrion on the outer side (Fig.9D). In the inner and outer interfaces, three and two pairs of contorted membranes were being synthesized respectively by fusion of DGV: among the three pairs of membranes, the outer and middle ones were the segments of ME and CHE respectively, while the inner one was likely the envelope of the next mitochondrion that appeared to be in preparation; likewise the two pairs of membranes were the outer side and inner side ME of the bulky and small mitochondria respectively (Fig.9D).

The above results demonstrated that mitochondrion was assembled in PC by encapsulating a selected portion of stroma with the membranes derived from PMT. As the assembly was nearly but not completely finished, CHE opened up at the ventral side of PC, allowing the detachment of mitochondrion and then resealed by incorporating CHE segment formed interior to the mitochondrion. Since mitochondria were always assembled in the ventral side of PC where a large nucleoid-like structure (NT) situated (Fig.9D), it was possible that mitochondrial DNA was synthesized in NT and subsequently sorted along with other constituents into mitochondria.

2.6 Biogenesis of vacuoles and degradation of PMT-derived vesicles

2.6.1 Mitochondria turned into vacuoles after matrix-degradation

Following the emergence of new mitochondrion, the opaque matrix of previously formed mitochondrion began to degrade into transparent material (Fig. 10A), such that the mitochondria turned into double-membrane-bounded vacuoles (V), containing ITB, IV and remnant CR, or only electron-transparent matrix (Fig. 10B). In parallel with vacuole biogenesis, a new mitochondrion was assembled within PC, two LD were developed at CE and a piece of chloroplast debris (CD) emerged in EM (Fig.10B). Hereafter, most ITB decomposed into electron-dense debris (ED) (Fig.10C), which was subsequently expelled outside into EM (Fig. 10D); while some ITB themselves also contained small ITB, so after degradation of their contents, the residual membranes (Fig. 10D) collected into MLB (Fig, 10 EF), resembling those in plant and animal cells (Dermaut et al., 2005; Paquet et al., 2013; Fernandez et al., 2013; Doorn et al; 2015).

Degradation of mitochondrial matrix was likely caused by the hydrolases released from CR; while the enzymes for ITB decomposition were presumably liberated from the space between its two limiting membranes, similar to the cases proposed for the transition of provacuole or autophagosome into vacuoles (Buvat and Robert, 1979; Marty 1999; Doorn and Papini, 2013) and double-membrane-bounded vacuoles (Aubert et al., 1996) in plant cells. Moreover, it was noteworthy that several cobblestone-shaped DRV appeared in EV (Fig.10F), confirming that PMT in PC was developed in a way similar to that of PT.

2.6.2 Formation and degradation of PMT-derived vesicles and coalescence of vacuoles

After vacuoles came into being, some short PMT in PC curled and ‘rolled up’ into “vesicle within vesicle” like compound vesicles (CPV) (Fig.11 ABC), which were taken up by vacuoles directly as they got segregated from PC (Fig. 11C), or after they shed into EM (Fig.11AB). After the internalized CPV released their contents for degradation, the remaining membranes stacked up into MLB (Fig. 11DEF). The vacuoles fused with each other by membrane protrusion. As shown in Fig. 11CD, a vacuole protruded into another one and fused at the contact sites, such that the membrane protrusion pinched off and became an IV (Fig.11E) or shed as MF (Fig. 11DF). When PC dwindled to a normal size, no more mitochondria and CPV were produced and all vacuoles coalesced into a large single one (Fig.11F). Hence, PC got matured into chloroplast (C) and as such PMT matured into eukaryotic thylakoids (T).

During vacuole biogenesis, cluster of SOV and tubules (TE) resembling the internal vesicle (body) of multivesicular body (Harding et al., 1983; Pan et al., 1985) was developed most likely from CD (Fig. 10B; Fig.11E) in the vicinity of nucleus or vacuoles (Fig.9C; Fig.11CDEF). CD

and VB (Fig.8A) were excised directly from PC, the latter of which was engulfed by PN. So, the content of CD was probably degraded by the enzymes released from nucleus, while the remaining PMT fragments coiled into SOV, part of which were internalized by vacuole and became IV (Fig.9D).

2.7 Vacuole mediated unconventional exocytosis and endocytosis

2.7.1 Vacuole-mediated unconventional exocytosis

Vacuoles came into contact and fused with CE, and then the fused membranes broke up into fragments resulting in large openings, from which a small quantity (Fig. 10DF; 12A) or a large amount of vacuolar content and SOV (Fig.12B) were expelled into ES. These expelled SOV were internalized from the neighboring SOV clusters (Fig.12B), which acted as exosomes (Johnstone et al., 1987; Théry et al., 2002) and perhaps transferred specific cargos to OM. Undoubtedly, the exocytotic materials contained proteins for remodeling the surface of CE and OM as well as thickening EW, which were sourced from PC, but not synthesized on endoplasmic reticulum (ER) and sorted through Golgi apparatus (GA) as did the normal secreted proteins (Rothman and Wieland, 1996; Schekman and Orci, 1996; Schatz and Dobberstein 1996). Therefore, the vacuole-mediated exocytosis was an unconventional (nonclassical) route of protein secretion (Nickel and Rabouille 2009; Zhang and Schekman, 2013; Ding et al., 2014; Robinson et al., 2016; Rabouille 2017). During exocytosis, the vacuolar membranes were apparently in vast excess of that required for cell expansion (Fig. 10DF; Fig.12AB), so the vacuole-mediated unconventional exocytosis released only a portion of the vacuolar content each time, more or less similar to the transient-fusion exocytosis (De Toledo et al., 1993) and open and closed exocytosis (Ren et al., 2016).

2.7.2 Vacuole-mediated unconventional endocytosis

The double-membranes of vacuole merged with CE at two distant sites and then invaginated, resulting in a large invaginated space (IVS), entrapping some electron-dense fibrils (EF) and globular particles (GP); while CE between the two merged sites disrupted and coiled into membranous structures (Fig.12C). Upon IVS reaching certain size, the membrane invagination pinched off into the vacuole lumen and became a large IV, whose content was degraded in situ or discharged into the vacuole lumen (Fig.12D). In the same way, the nascent vacuole also mediated small episode of endocytosis (Fig.10C). Evidently, the vacuole-mediated endocytosis was an unconventional endocytic route and distinct form the conventional endocytosis, where the small

endocytic vesicles passed their contents successively through the early endosome (trans-Golgi network) and late endosome (multivesicular body or pre-vacuolar compartments) for protein sorting and finally to the vacuole or lysosome for degradation (Blott and Griffiths 2002; Mayor and Pagano 2007; Saftig and Klumperman 2009; McMahon and Boucrot 2011; Chen et al., 2011; Fan et al., 2015). During this unconventional endocytic process, the vacuolar membranes were insufficient for IV development. Given that MLB presented in the vacuole with small invagination (Fig. 9D), but disappeared in the vacuole with large invagination Fig. 12C), it was possible that MLB served as membrane source for developing large IV.

2.8 Structure and reproduction of the TDX16-derived eukaryotic cell

2.8.1 Structure of the TDX16-derived eukaryotic cell

After bulk exocytosis and endocytosis, the large vacuoles disappeared, while the distorted thylakoids in the chloroplast straightened with narrowed luminal spaces (Fig.13ABC). As a result, the prokaryotic TDX16 cell (Fig.1-2) developed eventually into a stable eukaryotic cell with unique structure (Fig.13ABC). The TDX16-derived eukaryotic cell (TDX16-DE cell) was surrounded by an OM-containing EW, an ES of variable widths and a double-membraned CE, containing a characteristic “e-shaped” chloroplast, a nucleus with OE and NE, usually two mitochondria and frequently two or more small double-membrane-bounded vacuoles, but no EM, GA and peroxisomes (Fig.13ABC). Hence, OE, NE and CE served dual or multiple functions; while OM and ES consistently played similar roles as they did before organelle biogenesis (Fig. 1-6), though their composition and content apparently changed.

The large nucleus with no visible pores on OE and NE still contained a few RB (Fig.13ABC). When OE and NE became widely separated, some electron-dense vesicles (EDV) budded form NE into IES, and then fused with and re-budded from OE, ultimately migrated to the inner leaflet of CHE as well as the inner and outer leaflets of CE (Fig.13B), which probably delivered nucleus-synthesized proteins for maintaining the corresponding envelope membranes. During this process OE disrupted locally resulting in several openings, and more importantly, an opening was also formed at the contact site of OE and CE. Such that the proteins synthesized in EM could be sorted through OE openings into IES and then secreted via the opening on CE into ES (Fig. 13B). By contrast, when OE and NE came into contact, they fused at several sites and thus gave rise to openings, allowing nucleocytoplasmic transport (Fig.13C). Amazingly, a fusion pore was formed at the contact site of NE, OE and CE (Fig.13C), enabling the direct communication between nucleus and ES.

CE was the major site of lipid synthesis. As shown in (Fig.13C), three large and one nascent LD were assembled at CE inner membrane. Similar cases were frequently observed since the degradation of mitochondrion (Fig. 9BCD; Fig.10 BCDF; Fig.11 DEF; Fig.12AB). By contrast, LD was only occasionally formed at CHE (Fig.10C). Since OG was initially blistered from the CE outer membrane (CM), CE inner membrane (OIM) and IIM (Fig.1-3), these results demonstrated that CE was consistently the site of lipid synthesis; while OIM-derived CHE was also capable of lipid synthesis. Accordingly, EOV formed earlier were probably the primordial LD (Fig.6D; Fig.7ABF; Fig. 8CDF). In addition, EOB in NIC (Fig. 6D) and PC (Fig.7ABC; Fig.8D; Fig.12B) were perhaps analogous to LD, which seemed to be developed at PT and ST, similar to LD formation in the green alga (Fan et al., 2011; Goodson et al., 2011). So, EOB were likely packed into ITB of mitochondria and CPV, and subsequently expelled into EM in the form of LD (Fig.10E; Fig.11E).

EW, as described above (Fig. 7A), was consisted of a SH, an EL and an intervening OM (Fig.13B). Hence, ES was a membrane-surrounded compartment but not the extracellular space, which sequestered the liquid squeezing out from NX and likely served important functions in cell metabolism (Fig.7). Since ELV blistered consistently from OM into SH before (Fig.3-6), during (Fig.7-12) and after (Fig.13) organelle biogenesis, it was nearly certain that OM in EW was still the enzyme-anchoring site and responsible for assembling and modifying the external SH (Fig.3A). EL was likely perforated just as the original peptidoglycan layer (Fig.3A) allowing the passage and fusion of SOV and the like with OM.

2.8.2 Reproduction of TDX16-DE cell

TDX16-DE cell multiplied via autosporulation. As shown in Fig.13D, four autospores within an autosporangium (AUG) were segregated from each other by the wide interspace, more or less similar to the arrangement of TDX16 (endospores) in the sporangium (Fig.1). All these autospores contained a chloroplast of various sizes. In addition, the smallest autospore possessed a large nucleus, while the two large ones had mitochondrion and vacuoles and the last one had no other organelle at all. Hence, nucleus, mitochondrion and vacuole in most endospores were not allocated from the mother cell but developed from scratch. The presence of chloroplast but absence of mitochondrion in the same TDX16-DE cell suggested that the chloroplast thylakoids still retained respiratory electron transfer chains and were capable of oxidative phosphorylation, i.e., chlororespiration (Bennoun 1982; Peltier and Cournac 2002).

2.9 Photosynthetic pigments of TDX16 and TDX16-DE cell

In vivo absorption spectra (Fig.14A) showed that apart from the absorption maxima of chlorophyll a (Chl a) at 440 and 680 nm, TDX16 displayed a prominent peak at 630nm, corresponding to phycocyanin (PC) (Lemasson et al., 1973); while TDX16-DE cell exhibited a conspicuous shoulder peak of chlorophyll b (Chl b) at 653 nm (Govindjee and Rabinowitch, 1960), and a merged peak of carotenoids around 485 nm. Consistent with these results, fluorescence emission spectroscopy indicated that the water soluble pigment extract of TDX16 (Fig. 14E) and lipid soluble pigment extract of TDX16-DE (Fig. 14F) displayed an emission peak of PC at 646 nm (Gantt et al., 1979) and an emission peak of Chl b at 658 nm (Thorne et al., 1977) respectively, but no emission peak was detected in the water soluble pigment extract of TDX16-DE (Fig. 14E) and lipid soluble pigment extract of TDX16 (Fig. 14F). Furthermore, PC isolated from TDX16 had an absorption peak at 617nm (Fig. 14B), nearly the same as C–PC (Gantt et al., 1979); Chl b and lutein separating from TDX16-DE cell displayed absorption maxima at 456 and 645 nm (Fig. 14C), 420, 446 and 475nm (Fig. 14D) respectively, identical to those isolated from plants (Lichtenthaler, 1987).

2.10 16S rRNA sequences of TDX16 and TDX16-DE cell

16S rRNA sequence of TDX16 (GenBank KJ599678.2) was 98% identical with that of *Chroococcidiopsis thermalis* (GenBank NR102464.1) By contrast, 16S rRNA sequences of TDX16-DE chloroplast (GenBank KJ612008.1) showed high similarity of 99% to those of the chloroplasts of *Auxenochlorella protothecoides* (GenBank AY553213.1) and *Chlorella vulgaris* (GenBank AB001684.1).

2.11 Genome sequence of TDX16

TDX16 genome was 15,333,193 bp in size with an average of GC content of 55.21%, comprising 13,415 protein-coding genes, as well as 9 rRNA genes, 116 tRNA genes and 4 sRNA genes. This Whole Genome Shotgun project has been deposited at DDBJ/ENA/GenBank under the accession NDGV00000000. The version described in this paper is version NDGV01000000.

3. Discussion

The present study unveiled the biogenesis of chloroplast, nucleus, mitochondrion and vacuoles within the prokaryotic cell of TDX16. Consequentially, an essential question arose as to why this happened? Or what was the reason for organelle biogenesis in TDX16 cell?

The consistent results of cell structure (Fig.1-2), pigmentation (Fig.14) and 16S rRNA gene

sequence indicated that TDX16 was a PC-containing cyanobacterium resembling *C. thermalis*. However the genome size, gene number and GC content of TDX16 (GenBank NDGV00000000) were 2.43, 2.40 and 1.20 times those of *C. thermalis* (6,315,792 bp, 5593 genes and 44.4% GC) (GenBank CP003597.1) respectively. Since TDX16 was an endosymbiotic cyanobacterium released from the necrotic cell of green alga *H. pluvialis* (Dong et al., 2008; 2011), these results demonstrated that TDX16 had acquired at least 9,017,401bp DNA with 7822 genes from its host. Therefore, the reason for organelle biogenesis within TDX16 was the light-driven recombination (hybridization) and expression of the obtained eukaryotic genes and its own prokaryotic genes, the process of which was indicated by the changes of cell structures.

The obtained DNA was retained most likely in HGB, which contained DNA-like materials, situated in NU and remained a constant size in different cells (Fig.1). When compartmentalization commenced, the obtained DNA was released gradually from HGB into the NU (Fig. 3), most of which kept inactive because the initially formed PT were cyanobacterial ones, owing apparently to the expression of TDX16's own genes that were inhibited within the host cell (Fig.4). During the crucial re-compartmentalization, the total DNA in the solubilized ICP was gathered (Fig.5) and subsequently allocated into NS (major portion) and NIC (minor portion), where the obtained DNA and TDX16's own DNA began to recombine as indicated by the dismantling of PL and absence of PCB on the transitional PT-derived ST (Fig. 6). DNA-recombination quickly finished leading to the formation of PC sequestering the genes of chloroplast and mitochondrion and PN containing nucleus genes only (Fig.7). Thereafter, mitochondrial genome was assembled in PC and packed into mitochondria, while the remaining genes were organized into chloroplast genome (Fig. 8-11). So, it was not surprising that mitochondrial and chloroplast genomes shared similar features, and chloroplast genome retained some mitochondrion-related genes. The disappearance of PC (Fig. 14), PL (Fig. 7) and TDX16 16S rRNA, but appearance of 16S rRNA of TDX16-DE chloroplast indicated that DNA recombination involved the loss of some prokaryotic genes, but the synthesis new genes. Furthermore, the repartition of total DNA during re-compartmentalization (Fig. 6) inevitably resulted in the distribution of prokaryotic genes in nucleus genome and eukaryotic genes in chloroplast and mitochondrial genomes, giving the appearance of "gene transfer" or"DNA transfer" among different organelles.

In summary, aside from organelle biogenesis, the present study also revealed that (1) OG and PG were the precursors of thylakoids in cyanobacteria and chloroplast respectively; (2) LD formed mainly at CE and CHE; (3) MLB developed from ITB of mitochondrion and PMT-derived CPV; (4) exosomes (SOV) was derived from PC; (5) ES was a membrane-surrounded compartment and (6) EW was formed by modifying prokaryotic CW and contained an OM. Last but not the least,

organelle biogenesis in cyanobacterium TDX16 gave rise to a new green alga (TDX16-DE), which was the first instance of new species formation and demonstrated that a prokaryotic cell can acquire its eukaryotic host's genes and developed into a new eukaryotic cell. Therefore, the discovery of organelle biogenesis in TDX16 is of great importance and has profound effects on cell biology and evolutionary biology.

4. Materials and methods

4.1 Strain and culture

TDX16 was obtained from the necrotic and ruptured *H. pluvialis* cell (Dong et al., 2011) and maintained under low light intensity of 12 μmol photons m^{-2} s^{-1}, at 25 ℃ in the illumination incubator. For experiment, TDX16 was inoculated into sterilized 250-ml Erlenmeyer flasks containing 100 ml BG-11 medium (Stanier et al., 1971) and incubated under high light intensity of 60 μmol photons m^{-2} s^{-1}, at 25 ℃.

4.1 Microscopy preparations and observations

Cells were fixed with 2.5% glutaraldehyde and 1% osmium tetroxide, followed by dehydration with ascending concentrations of ethanol, and post staining with 3% uranyl acetate and lead citrate. The samples were examined with a JEM1010 electron microscope (JEOL, Japan).

4.2 Pigment analyses

4.2.1In vivo absorption spectra

Cell suspensions were scanned with Ultraviolet-Visible Spectrophotometer Cary 300 (Agilent, USA), the spectra were normalized to give an equal absorbance of Chl a at 440 nm.

4.2.2 Fluorescence emission spectra

Water soluble pigments were extracted with 0.75M K-phosphate buffer (pH=6.8). Lipid soluble pigments were extracted with pure acetone and diluted 50-fold into ethanol. Both extracts were analyzed directly on Fluorescence Spectrophotometer F-4500 (Hitachi, Japan) at room temperature with excitations of 580 and 478 nm respectively.

4.2.3 Pigment separation and identification

Chl b was separated by thin-layer chromatography according to the method described by

Lichtenthaler (Lichtenthaler, 1987). PC was extracted and purified following the procedures described by Adams (Adams et al., 1979). All pigments were analyzed with Ultraviolet-Visible Spectrophotometer Cary 300 (Agilent, USA), and identified by spectroscopic matching with the published data.

4.3 16S rRNA sequence

DNA samples were prepared according to the method described previously (Garcia-Pichel et al., 1998). 16S rRNAs were amplified using the primers 8-27f (AGAGTTTGATCCTGGCTCAG) and 1504-1486r (CTTGTTACGACTTCACCCC) (Moore et al., 1998). Fragments were cloned into the pMD18-T vector and amplified using M13 forward and reverse universal primers. The PCR products were digested with restriction enzymes BamH1/SalI, and sequenced on ABI 3730 DNA analyzer (PerkinElmer Biosystems, USA).

4.4 Genome sequence of TDX16

TDX16 cells were harvested by centrifugation at 3000 rpm for 10 min, and washed twice with 5M NaCl solution and sterile water alternately, with the pelleted cells being frozen in liquid nitrogen and then grinded with sterile glass beads (0.5 mm diameter).The slurry was transferred into 5ml centrifuge tube with TE buffer (1mM EDTA, 10 mM Tris-HCl, pH=8.0), supplemented with 1.0 ml lysozyme solution (20 mg/ml) and incubated at 37℃for 60 min, then added CTAB (Cetyltrimethyl ammonium bromide) solution (10% CTAB, 0.7 M NaCl) and heated to 65℃ for 30 min in a waterbath. After centrifugation (12000 rpm, 10min), the supernatant was extracted with one volume of phenol-chloroform-isoamyl alcohol (25:24:1, V/V), and DNA was precipitated overnight at −20 ℃ after the addition of 2/3 volume of cold isopropanol and 1/10 volume of 3M sodium acetate, dried and resuspended in TE buffer. The extracted DNA was first subjected to quality assay and then sheared ultrasonically into fragments, with their overhangs being converted into blunt ends applying T4 DNA polymerase, Klenow Fragment and T4 Polynucleotide Kinase. Subsequently, adapters were ligated to the 3' ends of DNA fragments that were introduced with ‘A’ bases. The obtained fragments were purified via gel-electrophoresis and PCR-amplified for preparing the sequencing library of DNA clusters. Paired-end sequencing was carried out on an IIlumina HiSeq 4000 platform, yeilding1.132 Mb raw data. After removal of the low quality reads, 1.009 Mb clean data was assembled with SOAPdenovo.

References

Abiodun, M.O and Matsuoka, K (2013) Evidence that proliferation of Golgi apparatus depends on both de novo generation from the endoplasmic reticulum and formation from pre-existing stacks during the growth of tobacco BY-2 cells. Plant Cell Physiol. 54: 541-554

Adams, S.M., Kao, O.W and Berns, D.S (1979) Psychrophile C-Phycocyanin. Plant Physiol. 64: 525–527.

Allen, M. M (1984) Cyanobacterial cell inclusions. Annu. Rev. Microbiol. 38:1-25.

Alvarez, H. M., Mayer, F., Fabritius, D., and Steinbüchel, A (1996) Formation of intracytoplasmic lipid inclusions by *Rhodococcus opacus* strain PD630. Arch. Microbiol. 165:377–386

Aseeva, E., Ossenbuhl, F., Sippel, C., et al. (2007) Vipp1 is required for basic thylakoid membrane formation but not for the assembly of thylakoid protein complexes. Plant Physiol. Biochem. 45: 119–128

Aubert, S., Gout, E., Bligny, R., Marty-Mazars, D., Barrieu, F., Alabouvette, J., Marty, F. and Douce, R (1996) Ultrastructural and biochemical characterization of autophagy in higher plant cells subjected to carbon deprivation: control by the supply of mitochondria with respiratory substrates. J. Cell Biol. 133: 1251–1263

Austin, J.R., Frost, E., Vidi, P.A., Kessler, F., and Staehelin, L.A (2006) Plastoglobules are lipoprotein subcompartments of the chloroplast that are permanently coupled to thylakoid membranes and contain biosynthetic enzymes. Plant Cell 18: 1693–1703

Barton, R (1965) Electron microscope studies on surface activity in cells of *Chara vulgaris*. Planta 66, 95—105

Berjak, P (1972) Lysosomal compartmentation: Ultrastructural aspects of the origin, development, and function of vacuoles in root cells of *Lepidium sativum*. Ann. Bot. (Lond.) 36: 73–81.

Bennoun P (1982) Evidence for a respiratory chain in the chloroplast. Proc. Natl. Acad. Sci. USA 79: 4352–4356

Beveridge, T. J (1999) Structure of Gram-negative cell walls and their derived membrane vesicles. J. Bcateriol. 181: 4725-4733

Bevis, B. J., Hammond, A. T., Reinke, C. A., and Glick, B. S (2002) De novo formation of transitional ER sites and Golgi structures in Pichia pastoris. Nature Cell Biol. 4, 750–756

Billi, D., Friedmann, E. I., Hofer, K.G., Caiola, M.G and Friedmann, R.O(2000) Ionizing-radiation resistance in the desiccation-tolerant cyanobacterium *Chroococcidiopsis*. Appl. Environ. Microbiol. 66:1489–1492

Blott, E. J. and Griffiths, G. M (2002) Secretory and lysosomes. Nat. Rev. Mol. Cell Biol. 3:122–131.

Brühlin, C., Kessler, F and van Wijk, K. J (2007) Plastoglobules: versatile lipoprotein particles in plastids. Trends plant sci. 12 (6):260-266

Brühlin, C and Kessler, F (2008) The plastoglobule: a bag full of lipid biochemistry tricks. Photochem. Photobiol. 84:1388–1394

Brown, D. L and Bisalputra, T (1969) Fine structure of the blue-green alga Nostoc sphaericum: the structured granule. Phycologia 8:119-126

Büdel, B and Rhiel, E (1985) A new cell wall structure in a symbiotic and free-living strain of the blue-green alga genus *Chroococcidiopsis* (Pleurocapsales). Arch. Microbiol. 143: 117-121.

Bullejahn, G. S and Sherman, L. A (1986) Identification of a Carotenoid-Binding Protein in the Cytoplasmic Membrane from the Heterotrophic Cyanobacterium *Synechocystis* sp. Strain PCC6714. J. Bacteriol. 167: 396-399

Buvat, R and Robert, G (1979) Vacuole formation in the actively growing root meristem of barley (Hordeum sativum). Am. J. Bot. 66:1219-1237

Caiola, M. G., Friedmann, R. C and Friedmann, E.I (1993) Cytology of long-term desiccation in the desert cyanobacterium *Chroococcidiopsis* (Chroococcales). Phycologia 32: 315-322.

Caiola, M.G., Billi, D and Friedmann, E. I (1996) Effect of desiccation on envelopes of the cyanobacterium *Chroococcidiopsis* sp. (Chroococcales). Eur. J. Phycol. 31:97–105.

Chen, X., Irani, N.G and Friml, J (2011) Clathrin-mediated endocytosis: the gateway into plant cells. Curr. Opin. Plant Biol. 14: 674–682

Cooley, J. W., and Vermaas, W. F. J (2001) Succinate dehydrogenase and other respiratory pathways in thylakoid membranes of *Synechocystis* sp. strain PCC 6803: capacity comparisons and physiological function. J. Bacteriol. 183: 4251–4258

Davidi, L., Levin, Y., Ben-Dor, S and Pick, U (2015) Proteome analysis of cytoplasmatic and plastidic b-carotene lipid droplets in *Dunaliella bardawil*. Plant Physiol. 167: 60–79

Dermaut, B., Norga, K.K., Kania, A., Verstreken, P., Pan, H. L., Zhou, Y., Callaerts, P and Bellen, H (2005) Aberrant lysosomal carbohydrate storage accompanies endocytic defects and neurodegeneration in *Drosophila benchwarmer*. J. Cell Biol. 170:127–139.

De Toledo, G. A., Fernandez-Chacon, R and Fernandez, J. M. (1993). Release of secretory products during transient vesicle fusion. Nature 363: 554–558.

Ding, Y., Wang, J., Wang, J.Q., Stierhof, Y. D., Robinson, D. G., and Jiang, L. W (2012) Unconventional protein secretion. Trends Plant Sci. 17:606-615.

Dong, Q. L., Li, Z.W., Xing, X.Y., Chen, B (2011) Discovery of an endophytic cyanobacterium in *Haematococcus pluvialis*. J. Hebei Univ.Technol. 40: 1-5

Edwards, M. R., Berns, D. S., Ghiorse, W.C., and Holt, S. C (1968) Ultrastructure of thermophilic

blue green alga *Synechococcus lividus* Copeland. J Phycol 4:283–298

Egan, A.J., Cleverley, R.M., Peters, K., Lewis, R.J., and Vollmer, W. (2016) Regulation of bacterial cell wall growth. FEBS J. 284: 851-867

Eltsov, M., and Zuber, B (2006) Transmission electron microscopy of the bacterial nucleoid. J. Struct. Biol. 156:246–54

Fan, J., Andre, C., and Xu, C (2011) A chloroplast pathway for the de novo biosynthesis of triacylglycerol in *Chlamydomonas reinhardtii*. FEBS Lett. 585:1985-1991.

Fan, L., Li, R., Pan, J., Ding, Z., and Lin, J (2015) Endocytosis and its regulation in plants. Trends Plant Sci. 20: 388-397

Fernández, M. C., Pérez-Gutierrez, M. A., Suarez-Santiago, V. N., Salinas-Bonillo, M. J., Romero-García, A. T (2013) Multilamellar bodies linked to two active plasmalemma regions in the pollen grains of *Sarcocapnos pulcherrima*. Biol. Plant. 57: 298-304.

Findley, D. L., Walne, P .L., and Holton, R.W (1970) The effects of light intensity on the ultrastructure of *Chlorogloea fritschii* mitra grown at high temperature. J. Phycol. 6: 182-188

Gantt, E., and Conti, S. F (1969) Ultrastructure of blue-green algae. J. Bacteriol. 97: 1486-1493

Gantt, E., Lipschultz, C. A., Grabowski, J., and Zimmerman, B .K. (1979) Phycobilisomes from blue-green and red algae: isolation criteria and dissociation characteristics. Plant Physiol. 63: 615–620.

Gao, H., and Xu, X (2009) Depletion of Vipp1 in *Synechocystis* sp. PCC 6803 affects photosynthetic activity before the loss of thylakoid membranes. FEMS Microbiol. Lett. 292: 63–70.

Garcia-Pichel, F., Nübel, U., and Muyzer, G (1998) The phylogeny of unicellular, extremely halotolerant cyanobacteria. Arch. Microbiol. 169, 469–482.

Gibbs, S.P (1962) The ultrastructure of the pyrenoids of green algae. J. Ultra. Res. 7: 262-272.

Glauert, A.M and Thornley M.J (1969) The topography of the bacterial cell wall. Annu. Rev. Microbiol. 23: 159–198.

Glick, B.S (2002) Can the Golgi form de novo? Nat. Rev. Mol. Cell Biol. 3:615–619.

Goodson, C., Roth, R., Wang, Z. T., Goodenough, U (2011) Structural correlates of cytoplasmic and chloroplast lipid body synthesis in *Chlamydomonas reinhardtii* and stimulation of lipid body production with acetate boost. Eukaryot. Cell 10:1592-1606.

Govindjee, and Rabinowitch, E (1960) Two forms of chlorophyll a in vivo with distinct photochemical functions. Science 132: 355-356.

Hansmann, P., and Sitte, P (1982) Composition and molecular structure of chromoplast globules of *Viola tricolor*. Plant Cell Rep. 1 : 111-114

Hay, E. D., and J. P. Revel (1963) The fine structure of the DNP component of the nucleus. J. Cell Biol. 16:29-51

Harding, C., Heuser, J., and Stahl, P (1983) Receptor-mediated endocytosis of transferrin and recycling of the transferrin receptor in rat reticulocytes. J. Cell Biol. 97:329–339.

Herman, E.M., Li, X., Su, R.T., Larsen, P., Hsu, H., and Sze, H (1994) Vacuolar-type H þ-ATPases are associated with the endoplasmic reticulum and provacuoles of root tip cells. Plant Physiol. 106: 1313–1324.

Hettema, E.H., and Gould, S. J (2017) Organelle formation from scratch. Nature, 542: 174-175

Hoepfner, D., Schildknegt, D., Braakman, I., Philippsen, P., and Tabak, H.F (2005) Contribution of the endoplasmic reticulum to peroxisome formation. Cell 122:85–95.

Hobot, J. A., Carlea, E., Villiger, W., and Kegenberger. E (1984) Periplasmic gel: new concept resulting from the reinvestigation of bacterial cell envelope ultrastructure by new methods. J. Bacteriol. 160:143-152.

Hoh, B., Hinz, G., Jeong, B. K., and Robinson, D.G (1995) Protein storage vacuoles form de novo during pea cotyledon development. J. Cell Sci. 108, 299-310

Hoiczyk, E., and Hansel, A (2000) Cyanobacterial cell walls: news from an unusual prokaryotic envelope. J. Bacteriol. 182: 1191-1199

Horowitz, R. A., Agard, D. A., Sedat, J. W., and Woodcock, C. L (1994) The three-dimensional architecture of chromatin in situ: Electron tomography reveals fibers composed of a continuously variable zig-zag nucleosomal ribbon. J. Cell Biol. 125:1–10

Huber, A., Koch, J., Kragler, F., Brocard, C., and Hartig, A (2012) A subtle interplay between three Pex11 proteins shapes de novo formation and fission of peroxisomes. Traffic 13: 157–167.

Huang, F., Perry, I., Nilsson, F., Parson, A. L., Pakrasi, H. B., Andersson, B., and Norling B (2002) Proteomics of *Synechocystis* sp. strain PCC 6803: identification of plasma membrane proteins. Mol. Cell Proteomics 1:956–966

Kalscheuer, R., Stöveken, T., Malkus, U., Reichelt, R., Golyshin, P. N., Sabirova, J. S., Ferrer, M., Timmis, K. N., Steinbüchel, A (2007) Analysis of storage lipid accumulation in *Alcanivorax borkumensis*: evidence for alternative triacylglycerol biosynthesis routes in bacteria. J. Bacteriol. 189: 918–928.

Kornfeld, S., and Mellman, I (1989) The biogenesis of lysosomes. Annu. Rev. Cell Biol. 5, 483-525.

Keren, N., Liberton, M., and Pakrasi, H. B (2005) Photochemical competence of assembled

photosystem II core complex in cyanobacterial plasma membrane. J. Biol. Chem. 280: 6548–6553

Kim, P. K., Mullen, R. T., Schumann, U., and Lippincott-Schwartz, J (2006) The origin and maintenance of mammalian peroxisomes involves a de novo PEX16-dependent pathway from the ER. J. Cell Biol. 173: 521–532

Jian, Q. U., Zhang, C. M., and Zhai, Z. H (1994) Observation of nuclei reassembled from demembranated Xenopus sperm nuclei and analysis of their lamina components. Cell Res. 4: 163–172

Johnstone, R. M., Adam, M., Hammond, J. R., Orr, L., and Turbide, C (1987) Vesicle formation during reticulocyte maturation. Association of plasma-membrane activities with released vesicles (exosomes). J. Biol. Chem. 262: 9412–9420

Jürgens, U. J., and Weckesser, J (1985) Carotenoid-containing outer membrane of *Synechocystis* sp. strain PCC 6714. J. Bacteriol. 164:384–389.

Lang, N. J (1968) The fine structure of blue-green algae. Ann. Rev. Microbiol. 22: 15-46.

Lang, N. J., and Fisher, K. A (1969) Variation in the fixation image of "structural granules" in *Anabaena*. Arch. Mikrobiol. 67: 173—181

Lea-Smith, D. L., Ross, N., Zori, M., Bendall, D. S., Dennis, J. S., Scott, S. A., Smith, A. G., Howe, C. G (2013) Thylakoid terminal oxidases are essential for the cyanobacterium *Synechocystis* sp. PCC6803 to survive rapidly changing light intensities. Plant Physiol. 162:484–495.

Lemasson. C., Marsac, N. T., and Cohen-Bazire, G (1973) Role of allophycocyanin as a light-harvesting pigment in cyanobacteria. Proc. Nat. Acad. Sci. USA 70: 3130-3133.

Li, H. M., Kaneko, Y., and Keegstra, K (1994) Molecular cloning of a chloroplastic protein associated with both the envelope and thylakoid membranes. Plant Mol. Biol. 25: 619–632.

Li, Y., Xu, M., Ding, X., Yan, C., Song, Z., Chen, L., Huang, X., Wang, X., Jian, Y., Tang, G., Tang, C., Di, Y., Mu, S., Liu, X., Liu, K., Li, T., Wang, Y., Miao, L., Guo, W., Hao, X., Yang, C (2016) Protein kinase C controls lysosome biogenesis independently of mTORC1. Nat Cell Biol. 18:1065–1077.

Liberton, M., Berg, R. H., Heuser, J., Roth, R., and Pakrasi, H. B (2006) Ultrastructure of the membrane systems in the unicellular cyanobacterium *Synechocystis* sp strain PCC 6803. Protoplasma 227: 129–138

Lichtenthaler, H. K(1987) Chlorophylls and carotenoids: pigments of photosynthetic biomembranes. Methods Enzymol. 148, 350–382.

Lichtenthaler, H. K (2013) Plastoglobuli, thylakoids, chloroplast structure and development of

plastids. In: Biswal B, Krupinska K, Biswal UC (eds) Plastid development in leaves during growth and senescence advances in photosynthesis and respiration. Springer, Berlin, pp 337–361.

Liu, D. F., Xu, L., Yang, F., Li, D.D., Gong, F.L. and Xu, T (2005) Rapid biogenesis and sensitization of secretory lysosomes in NK cells mediated by target-cell recognition. Proc. Natl. Acad. Sci. USA. 102:123–127.

Lokha, M. J., and Masui, Y (1983) Formation in vitro of sperm pronuclei and mitotic chromosomes induced by amphibian ooplasmic components. Science 220:719-21.

Lowe, M and Barr, F. A (2007) Inheritance and biogenesis of organelles in the secretory pathway. Nat. Rev. Mol. Cell. Biol. 8:429–439.

Luzio, J. P, Hackmann, Y., Dieckmann, N. M., Griffiths, G. M (2014) The biogenesis of lysosomes and lysosome-related organelles. Cold Spring Harb. Perspect. Biol. 6(9):a016840

Marty, F (1978) Cytochemical studies on GERL, provacuoles, and vacuoles in root meristematic cells of Euphorbia. Proc. Natl. Acad. Sci. USA 75: 852–856.

Marty, F (1999) Plant vacuoles. Plant Cell 11:587-600

Mayor, S., and Pagano, R. E (2007) Pathways of clathrin-independent endocytosis. Nat. Rev. Mol. Cell Biol. 8: 603–612

McMahon, H. T., and Boucrot, E (2011) Molecular mechanism and physiological functions of clathrin-mediated endocytosis. Nat. Rev. Mol. Cell Biol. 12: 517–533

Meindl, U., Lancelle, S., and Hepler, P. K (1992) Vesicle production and fusion during lobe formation in Micrasterias visualized by high-pressure freeze fixation. Protoplasma 170:104--114

Moore, L. R., Rocap, G., and Chisholm, S. W (1998). Physiology and molecular phylogeny of coexisting *Prochlorococcus* ecotypes. Nature 393: 464–467.

Motley, A. M., and Hettema, E. H (2007) Yeast peroxisomes multiply by growth and division. J. Cell Biol. 178: 399–410

Mullineaux, C. W (2014) Co-existence of photosynthetic and respiratory activities in cyanobacterial thylakoid membranes. Biochim. Biophys. Acta 1837: 503–511

Newport, J (1987) Nuclear reconstitution in vitro: Stages of assembly around protein-free DNA. Cell 48:205-217

Nickel, W., and Rabouille, C (2009) Mechanisms of regulated unconventional protein secretion. Nat. Rev. Mol. Cell Biol. 10:234-255

Olbrich, A., Hillmer, S., Hinz, G., Oliviusson, P., Robinson, D. G (2007) Newly formed vacuoles in root meristems of barley and pea seedlings have characteristics of both protein storage

and lytic vacuoles. Plant Physiol. 145:1383-1394.

Opaliński, Ł., Bartoszewska, M., Fekken, S., Liu, H., de Boer, R., et al. (2012) De novo peroxisome biogenesis in *Penicillium chrysogenum* is not dependent on the Pex11 family members or Pex16. PLoS ONE 7: e35490. doi:10.1371/journal.pone.0035490

Osborn, M. J., Gander, J. E., Parisi, E., and Carson, J (1972) Mechanism of assembly of outer membrane of *Salmonella typhimurium*: Isolation and characterization of cytoplasmic and outer membrane. J. Biol. Chem. 247:3962-3972.

Packter, N. M., and Olukoshi, E. R (1995) Ultrastructural studies of neutral lipid localisation in Streptomyces. Arch. Microbiol. 164:420–427

Pan, B.T., Teng, K., Wu, C., Adam, M., and Johnstone, R.M (1985) Electron microscopic evidence for externalization of the transferrin receptor in vesicular form in sheep reticulocytes. J. Cell Biol. 101:942-948

Paquet, V.E., Lessire, R., Domergue, F., Fouillen, L., Filion, G., Sedighi, A., Charette, S.J (2013) Lipid composition of multilamellar bodies secreted by *Dictyostelium discoideum* reveals their Amoebal origin. Eukaryotic Cell 12: 1326–1334.

Peltier, G., and Cournac, L (2002) Chlororespiration. Annu. Rev. Plant Biol. 53: 523–550.

Peramuna, A., and Summers, M. L (2014) Composition and occurrence of lipid droplets in the cyanobacterium *Nostoc punctiforme*. Arch. Microbiol. 196: 881–890

Perera, R. M., and Zoncu, R (2016) The lysosome as a regulatory hub. Annu. Rev. Cell Dev. Biol. 32: 223–253

Peschek, G.A., Hinterstoisser, B., Wastyn, M., Kuntner, O., Plneau, E., Missblchler, A., and Lang, J (1989) Chlorophyll precursors in the plasma membrane of a cyanobacterium *Anacystis nidulans*. J. Biol. Chem. 264: 11827-11832.

Rabouille, C (2017) Pathways of unconventional protein secretion. Trends Cell Biol. 27:230–240

Ren, L., Mellander, L., Keighron, J., Cans, A. S., Kurczy, M., Svir, I., Oleinick, A., Amatore, C., Ewing, A. G (2016) The evidence for open and closed exocytosis as the primary release mechanism. Q. Rev. Biophys. 49, e12.

Robinson, D.G., Ding, Y., and Jiang L. W (2016) Unconventional protein secretion in plants: a critical assessment. Protoplasma 253: 31–43

Resch, C. M., and J. Gibson (1983) Isolation of the carotenoid-containing cell wall of three unicellular cyanobacteria. J. Bacteriol. 155:345-350.

Rexroth, S., Mullineaux, C. W., Ellinger, D., Sendtko, E., Rögner, M., and Koenig, F (2011) The plasma membrane of the cyanobacterium *Gloeobacter violaceus* contains segregated bioenergetic domains. Plant Cell 23: 2379–2390.

Rippka, R., Waterbury, J., and Cohen-Bazire, G (1974) A cyanobacterium which lacks thylakoids. Arch. Microbiol. 100: 419–436.

Robinow, C., and Kellenberger, E (1994) The bacterial nucleoid revisited. Microbiol. Rev. 58:211–232.

Rothman, J. E., and Wieland, F. T (1996) Protein sorting by transport vesicles. Science 272: 227–234.

Rossanese, O. W., Soderholm, J., Bevis, B. J., Sears, I. B., O'Connor, J., Williamson, E. K., and Glick, B. S (1999) Golgi structure correlates with transitional endoplasmic reticulum organization in *Pichia pastoris* and *Saccharomyces cerevisiae*. J. Cell Biol. 145:69–81

Rucktaschel, R., Halbach, A., Girzalsky, W., Rottensteiner, H., and Erdmann, R (2010) De novo synthesis of peroxisomes upon mitochondrial targeting of Pex3p. Eur. J. Cell Biol. 89, 947–954

Saftig P., and Klumperman, J (2009) Lysosome biogenesis and lysosomal membrane proteins: trafficking meets function. Nat. Rev. Mol. Cell Biol. 10: 623–635

Samuels, A. L., Giddings, T. H., and Staehelin, L. A (1995) Cytokinesis in tobacco BY-2 and root tip cells: a new model of cell plate formation in higher plants. J. Cell Biol. 130: 1345–1357

Schatz, G., and Dobberstein, B (1996) Common principles of protein translocation across membranes. Science 271:1519–1526.

Schekman, R., and Orci, L (1996) Coat proteins and vesicle budding. Science 271: 1526–1533.

Shively, J. M., Ball, F., Brown, D. H., and Saunders, R. E (1973) Functional organelles in prokaryotes: polyhedral inclusions (carboxysomes) of *Thiobacillus neapolitanus*. Science 182: 584–586

Simon, R. D (1971) Cyanophycin granules form the blue-green alga *Anabaena cylindrica*: a reserve material consisting of copolymers of aspartic acid and arginine. Proc. Natl. Acad. Sci. USA 68:265–267.

Smith, D., and Howe, C. J (1993) The distribution of Photosystem I and Photosystem II polypeptides between the cytoplasmic and thylakoid membranes of cyanobacteria. FEMS Microbiol. Lett. 110: 341-348

Smith, M. D., Licatalosi, D. D., and Thompson, J. E (2000) Co-association of cytochrome f catabolites and plastid-lipid-associated protein with chloroplast lipid particles. Plant Physiol. 124: 211–222

South, S. T., and Gould, S. J (1999) Peroxisome Synthesis in the Absence of Preexisting Peroxisomes. J. Cell Biol. 144: 255–266

Srivastava, R., Battchikova, N., Norling, B., and Aro, E.M (2006) Plasma membrane of

Synechocystis PCC 6803: A heterogeneous distribution of membrane proteins. Arch. Microbiol. 185: 238–243.

Stanier, R. Y., Kunisawa, R., Mandel, M., and Cohen-Bazire, G. (1971). Purification and properties of unicellular blue-green algae (Order Chroococcales). Bacteriol. Rev. 35: 171-205.

Sugiura, A., Mattie, S., Prudent, J., and McBride, H. M (2017) Newly born peroxisomes are a hybrid of mitochondrial and ER-derived pre-peroxisomes. Nature 542: 251–254

Tängemo, C., Ronchi, P., Colombelli, J., Haselmann, U., Simpson, J.C., Antony, C., Stelzer, E.H.K., Pepperkok, R., and Reynaud, E.G (2010) A novel laser nanosurgery approach supports de novo Golgi biogenesis in mammalian cells. J. Cell Sci. 124: 978-987

Théry, C., Zitvogel, L., and Amigorena, S (2002) Exosomes: composition, biogenesis and function. Nat. Rev. Immunol. 2: 569-579

Thorne, S.W., Newcomb, E.H., and Osmond, C.B (1977) Identification of chlorophyll b in extracts of prokaryotic algae by fluorescence spectroscopy. Proc. Natl. Acad. Sci. USA 74: 575–578.

van der Zand, A., Gent, J., Braakman, I., and Tabak, H. F (2012) Biochemically distinct vesicles from the endoplasmic reticulum fuse to form peroxisomes. Cell 149: 397–409.

van de Meene, A. M., Hohmann-Marriott, M. F., Vermaas, W. F., Roberson, R. W (2006) The three-dimensional structure of the cyanobacterium *Synechocystis* sp. PCC 6803. Arch. Microbiol. 184: 259–270

van Doorn, W. G., Kirasak, K., and Ketsa, S (2015) Macroautophagy and microautophagy in relation to vacuole formation in mesophyll cells of *Dendrobium tepals*. J. Plant Physiol. 177: 67–73

van Doorn, W. G., and Papini, A (2013) Ultrastructure of autophagy in plant cells. Autophagy 9:1922-1936

Vidi, P., Kanwischer, M., Baginsky, S., Austin, J. R., Csucs, G., Dörmann, P., Kessler, F., and Bréhélin, C (2006) Tocopherol cyclase (VTE1) localization and vitamin E accumulation in chloroplast plastoglobule lipoprotein particles. J. Biol. Chem. 281: 11225–11234

Vigers, G. P., and Lohka, M. J (1991) A distinct vesicle population targets membranes and pore pomplexes to the nuclear envelope in Xenopus eggs. J. Cell Biol. 112, 545–556.

Viotti, C., et al. (2013) The endoplasmic reticulum is the main membrane source for biogenesis of the lytic vacuole in *Arabidopsis*. Plant Cell 25:3434–3449.

Waterbury, J. B., and Stanier, R. Y (1978) Patterns of growth and development in Pleurocapsalean cyanobacteria. Microbiol. Rev. 42: 2-44

Westphal, S., Heins, L., Soll, J., and Vothknecht, U. C (2001) Vipp1 deletion mutant of

Synechocystis: a connection between bacterial phage shock and thylakoid biogenesis? Proc. Natl. Acad. Sci. USA 98: 4243–4248.

Yeates, T. O., Kerfeld, C. A., Heinhorst, S., Cannon, G. C., and Shively, J. M (2008) Protein-based organelles in bacteria: carboxysomes and related microcompartments. Nat. Rev. Microbiol. 6: 681–691

Ytterberg, A. J., Peltier, J., and van Wijk, K. J (2006) Protein profiling of plastoglobules in chloroplasts and chromoplasts. A surprising site for differential accumulation of metabolic enzymes. Plant Physiol. 140: 984–997

Zak, E., Norling, B., Maitra, R., Huang, F., Andersson, B., and Pakrasi, H. B (2001) The initial steps of biogenesis of cyanobacterial photosystems occur in plasma membranes. Proc. Natl. Acad. Sci. USA 98:13443–13448

Zhang, M., and Schekman, R (2013) Cell biology. Unconventional secretion, unconventional solutions. Science 340:559-561.

Zhang, S., Shen, S., Li, Z., Golbeck, J. H., and Bryant, D.A (2014) Vipp1 is essential for biogenesis of Photosystem I but not thylakoid membranes in *Synechococcus* sp. PCC7002. J. Biol. Chem. 289: 15904–15914.

Acknowledgements

This work was supported by the Natural Science Foundation of Hebei Province (B2008000029).

Author contributions

Q.L.D and X.Y.X. performed the experiment and wrote the manuscript with the participation of Y.H in partial electron microscopic observation and 16S rRNA sequencing, X.L.W and S. Z in pigment analyses.

List of abbreviations

AUG	Autosporangium
C	Chloroplast
CD	Chloroplast debris
CE	Cytoplasmic envelope
CF	Chromatin fibers
CG	Cyanophycin granules
CHE	Chloroplast envelope
CLM	Cloudlike materials
CM	Cytoplasmic membrane
CPV	Compound vesicles
CR	Cristae
CV	Combined vesicles
CW	Cell wall
CX	Carboxysomes
DF	DNA Fibers
DGV	Dense-margined vesicles
DLF	DNA-like fibrils
DMF	Double-layered membrane fragment
DMS	Double-layered membrane segment
DMV	Double-membraned vesicles
DRV	Dilated ring-shaped vesicles
DSV	Dense vesicle
DT	DNA threads
DV	Dotted vesicles
ED	Electron-dense debris
EDV	Electron-dense vesicles
EF	Electron-dense fibrils
EG	Electron-dense granules
EIS	Empty Inner space
EL	Electron-dense layer
ELM	Electron-translucent materials
ELV	Electron-translucent vesicles
EM	Eukaryotic cytoplasm
EOB	Electron-opaque bodies
EOP	Electron-opaque particles
EOM	Electron-opaque materials
EOV	Electron-opaque vesicles
EP	Electron-dense particles
EPM	Electron-transparent materials
ER	Endoplasmic reticulum
ES	Extracytoplasmic space
EV	Electron-transparent vesicle
EW	Eukaryotic cell wall
FM	Fibrillary materials
GA	Golgi apparatus
GP	Globular particles
HGB	Heterogenous globular bodies
IB	Intranuclear body
ICE	Intracytoplasmic envelope
ICP	Inner cytoplasm
IES	Inter envelope space
IIM	Inner intracytoplasmic membrane
IIS	Inner intracytoplasmic space
INS	Interspace
IS	Intracytoplasmic space
ITB	Internal body
IV	Internal vesicle
IVS	Invaginated space
LD	Lipid droplet
LDB	Less electron-dense bodies
LDM	Less electron-dense materials
LM	Limiting membrane
M	Mitochondrion
ME	Mitochondrial envelope
MF	Membrane fragments
ML	Microfibrils
MLB	Multilamellar body
MR	Margin residues
MS	Membrane segments
MT	Membranous elements
MV	Microvesicles
N	Nucleus
NE	Nuclear envelope
NIC	New inner cytoplasm
NIS	New inner intracytoplasmic space
NS	New intracytoplasmic space
NT	Nucleoid-like structure
NU	Nucleoid
NX	New intracytoplasmic matrix
OCP	Outer cytoplasm
OE	Outer nuclear envelope
OG	Osmiophilic granules
OIM	Outer intracytoplasmic membrane
OIS	Outer intracytoplasmic space

OPV	Opaque-periphery vesicle	SA	Sporangium
OM	Outer membrane	SG	Starch granules
OV	Oblong vesicles	SH	Sheath
P	Peptidoglycan layer	SMV	Smaller vesicles
PB	Polyphosphate bodies	SM	Stroma
PC	Primitive chloroplast	SOV	Small opaque vesicle
PCB	Phycobilisomes	SP	Starch plate
PD	Pyrenoids	ST	Secondary thylakoids
PG	Plastoglobuli	SV	Small vesicles
PL	Peptidoglycan-like layer	T	Thylakoids
PMT	Primitive thylakoids	TE	Tubules
PN	Primitive nucleus	TL	Thylakoid-like structure
PNE	Primitive nuclear envelope	TMF	Two-layered membrane fragment
PO	Pores	TMV	Thick margin vesicle
PT	Primary thylakoids	TV	Tiny vesicles
RB	Ribosomes	V	Vacuole
RM	Residual membranes	VB	Vesicle-containing body
RV	Ring-shaped vesicles		

Figures

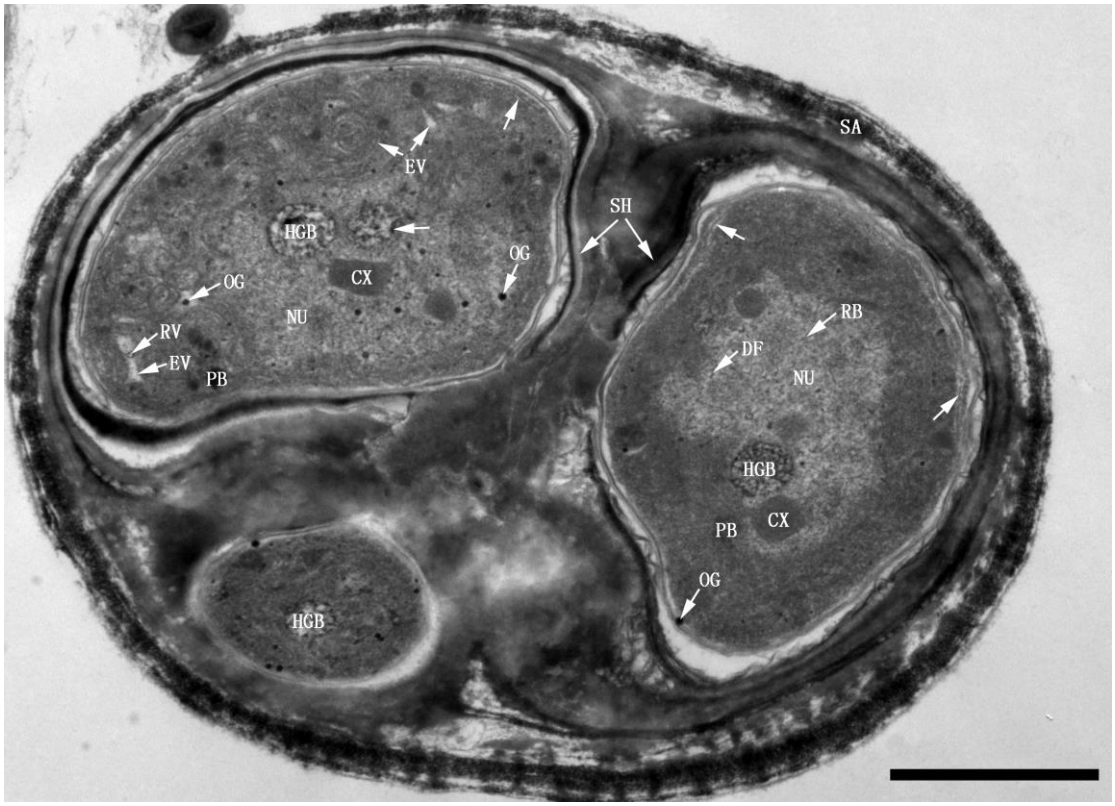

Figure1. Three TDX16 cells within a sporangium (SA). TDX16 cells were enclosed by thick sheaths (SH), containing no organelle and thylakoid, but unique heterogenous globular bodies (HGB), carboxysomes (CX), ribosomes (RB), DNA fibers (DF) and osmiophilic granules (OG) in the nucleoids (NU) as well as polyphosphate bodies (PB) in the cytoplasm. OG also presented in cytoplasm and some small electron-transparent vesicles (EV) with internal ring-shaped vesicles (RV) or OG were being formed in the upper left cell. Compartmentalization was just initiated in the two large cells (arrow). Scale bar, 1μm.

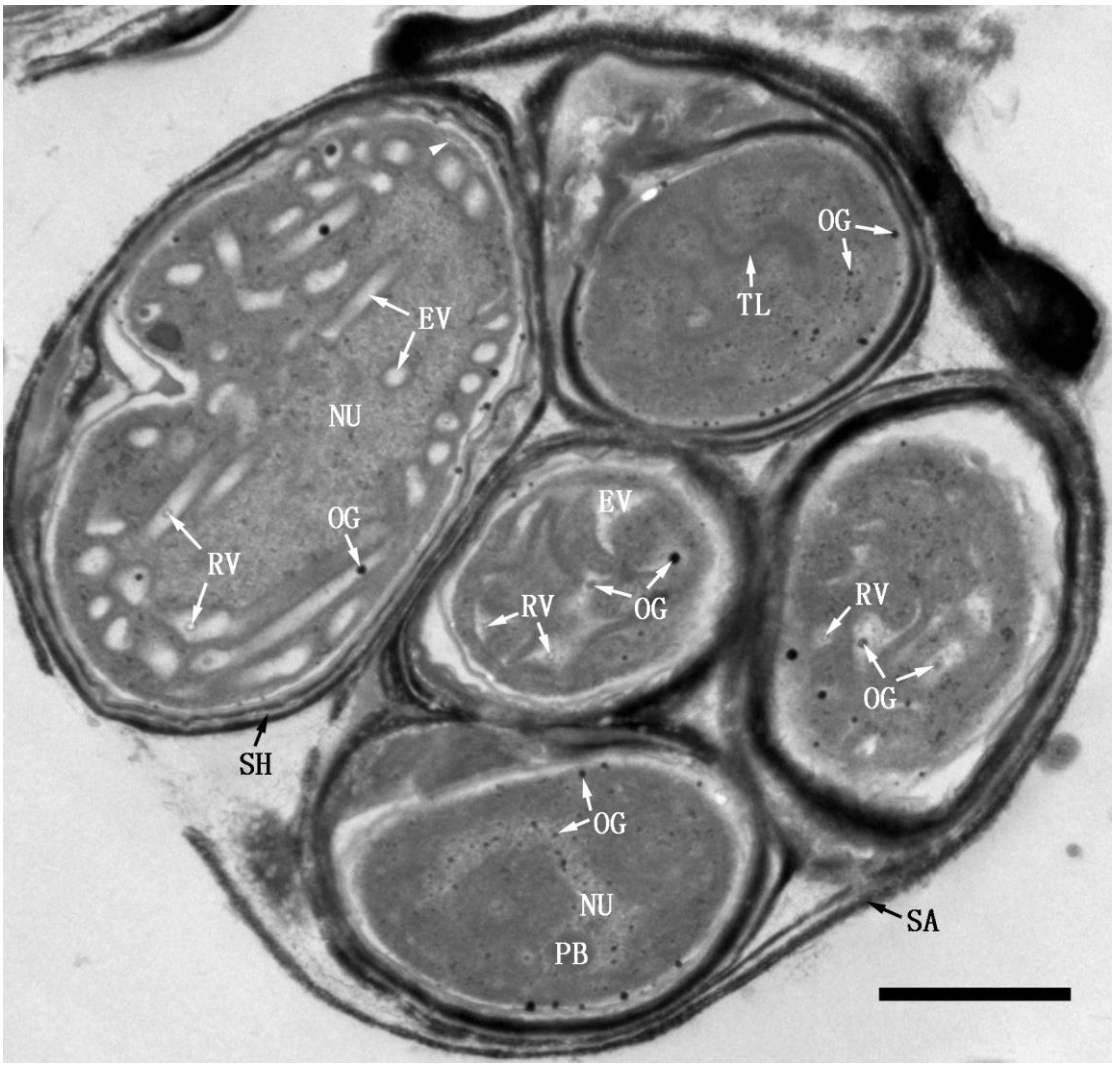

Figure 2. Five TDX16 cells within a SA. The bottom cell was devoid of EV, while a great number of EV were being developed in the three middle cells, and several thylakoid-like structures (TL) were built up in the upper cell. Compartmentalization commenced in the large cell (arrowhead). Scale bar, 1μm.

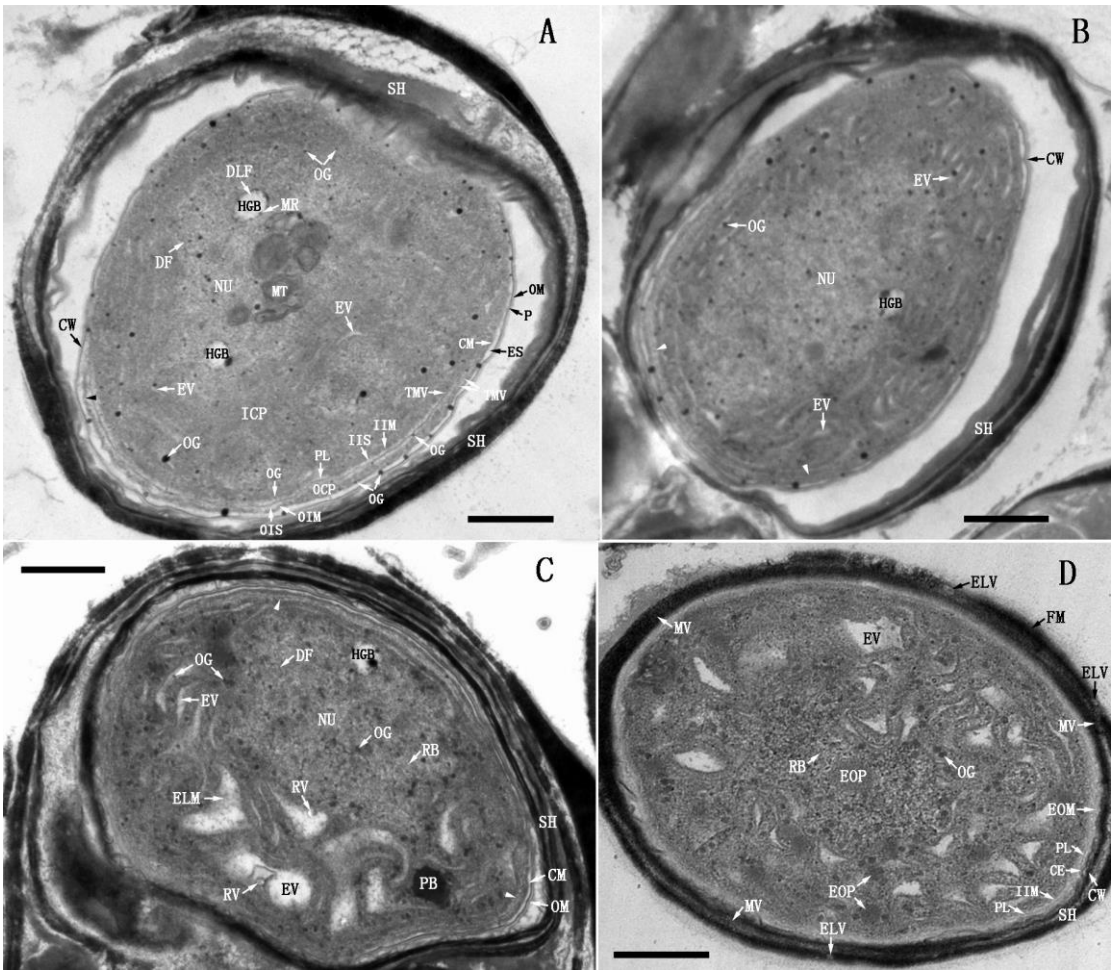

Figure 3. Compartmentalization, formation of EV and cytoplasmic envelope. (**A**) TDX16's cell wall (CW) comprised an outer membrane (OM) and a peptidoglycan layer (P), which was separated from the cytoplasmic membrane (CM) by an extracytoplasmic space (ES). Inside the cytoplasm, an inner intracytoplasmic membrane (IIM), an outer intracytoplasmic membrane (OIM) and an intervening peptidoglycan-like layer (PL) were being synthesized by fusion of the small thick margin vesicles (TMV) blistered form the inner leaflet of the cytoplasmic membrane. Whereby, the cytoplasm was partitioned into three compartments: the inner cytoplasm (ICP); the outer cytoplasm (OCP), and the sandwiched intracytoplasmic space (IS) that was further separated by PL into an outer intracytoplasmic space (OIS) and an inner intracytoplasmic space (IIS). OCP began to reduce in localized region near the start point (arrowhead), such that OIM moved to CM. OG budded from the inner leaflet of CM, IIM and OIM, and migrated into ICP, where many small EV were being formed and stacks of membranous elements (MT) emerged; while HGB became nearly empty leaving only DNA-like fibrils (DLF) and electron-dense margin residues (MR). Interestingly, OG shed from the outer leaflet of CM into ES, connecting CM and CW. (**B**) IS became narrow (arrow), while more and more small EV were being developed from OG. (**C**) EV dilated into swirling ones spiraling around NU, but IS still remained narrow. (**D**) When EV was formed in NU, several electron-opaque particles (EOP) emerged, while IS became widened filling with electron-opaque materials (EOM). Importantly, OCP disappeared such that OIM and CM were positioned together, and became a double-membraned cytoplasmic envelope (CE). Some electron-dense materials were synthesized on CE and transferred to CW for assembling SH, which was made up of flocculent fibrillary materials (FM), microvesicles (MV) and electron-translucent vesicles (ELV). Scale bar, 0.5 μm.

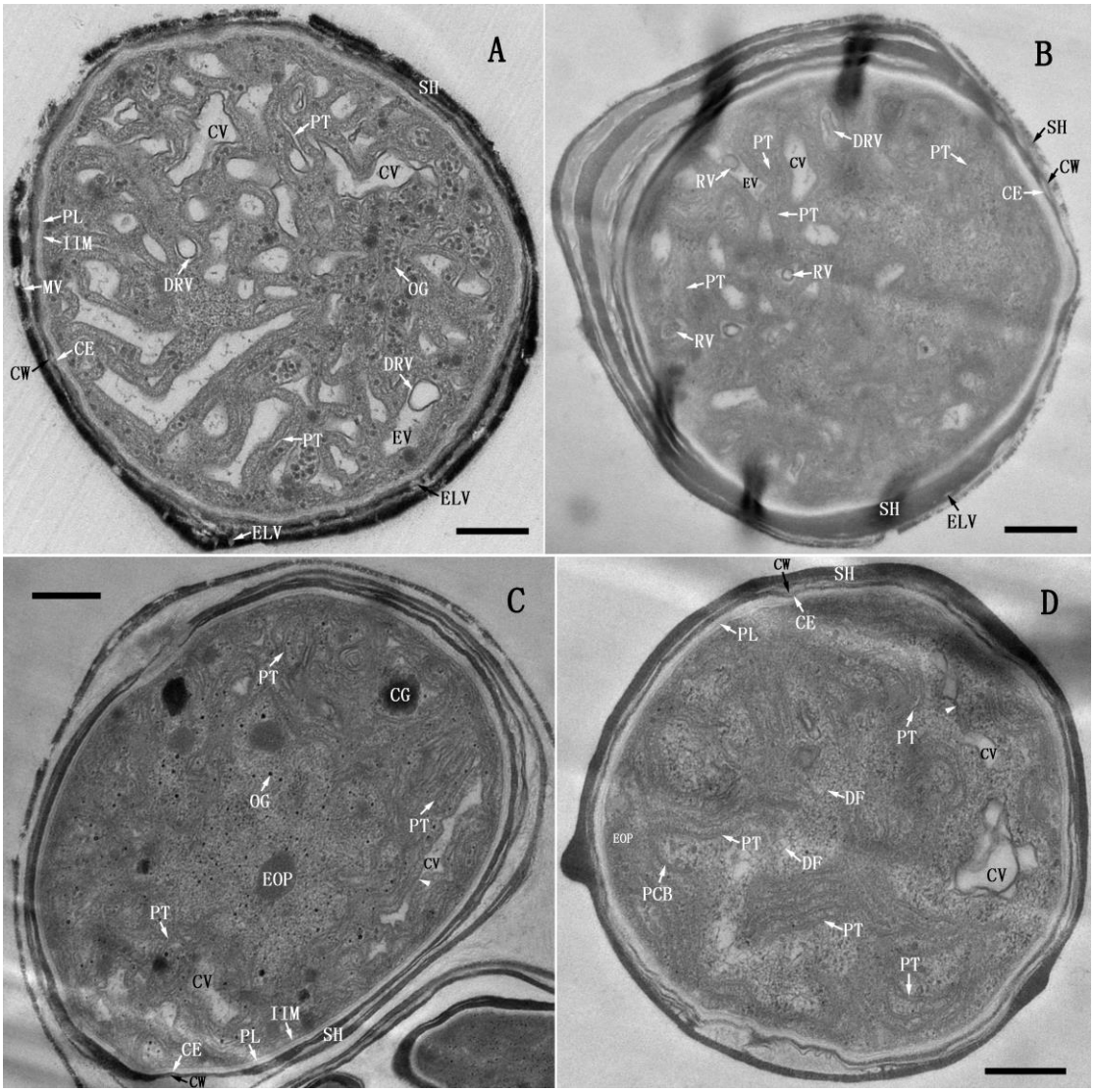

Figure 4. Development of EV into primary thylakoid. (**A**) RV swelled into dilated-ring-shaped vesicle (DRV), whose membrane met ultimately with EV membrane, and thus gave rise to a unit-membrane-bounded combined vesicle (CV). Subsequently, CV coalesced into longer ones or flattened out into slender short primary thylakoids (PT). (**B**) The newly formed short PT distributed randomly in ICP, whose matrix turned opaque. Occasionally a cluster of small RV presented in a EV. (**C**) The short PT extended or merged end-to-end into long PT; while the long coalesced CV flattened out into PT by localized-constriction (arrowhead).Meanwhile, several cyanophycin granules (CG) were formed. (**D**) PT became parallel-arranged with wide spacing, on which the extrinsic phycobilisomes (PCB) were assembled. Scale bar, 0.5 μm.

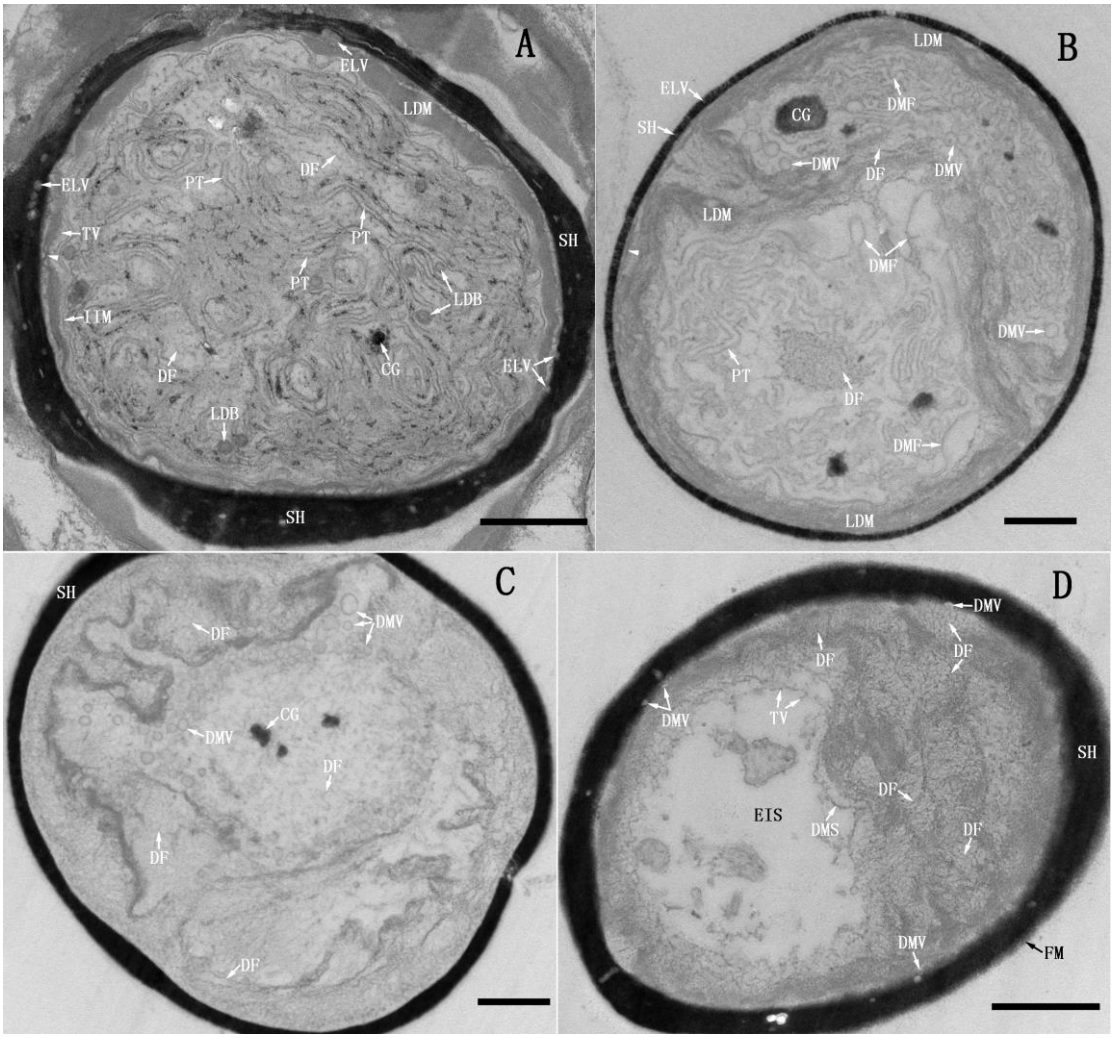

Figure 5. Decondensation of ICP, disassembly of IIM and PT, and translocation of DNA. (**A**) IIM broke down and rounded up into tiny vesicles (TV); PT matrix condensed and thus the membrane pair were in close apposition with concurrent disassembly of PCB; ICP decondensed and became translucent, in which short DF dispersed, and some less electron-dense materials (LDM) and less electron-dense bodies (LDB) were formed. LDM diffused outward and blurred the compacted PL, CE and CW (arrowhead). (**B**) PT broken up into double-layered membrane fragments (DMF), which began to merge laterally into double-membraned vesicles (DMV); while DF aggregated into a cluster. (**C**) All PT transformed into DMV, dispersing along with the aggregated DNA fibers in the decondensed ICP. (**D**) DMV moved outward quickly and attached to PL that was cover by electron-dense materials, while the intermingled DF scattered outward slowly resulting in an "empty" inner space (EIS), at the border of which the recruited TV began to fuse and elongate into double-layered membrane segments (DMS). Scale bar, 0.5 μm.

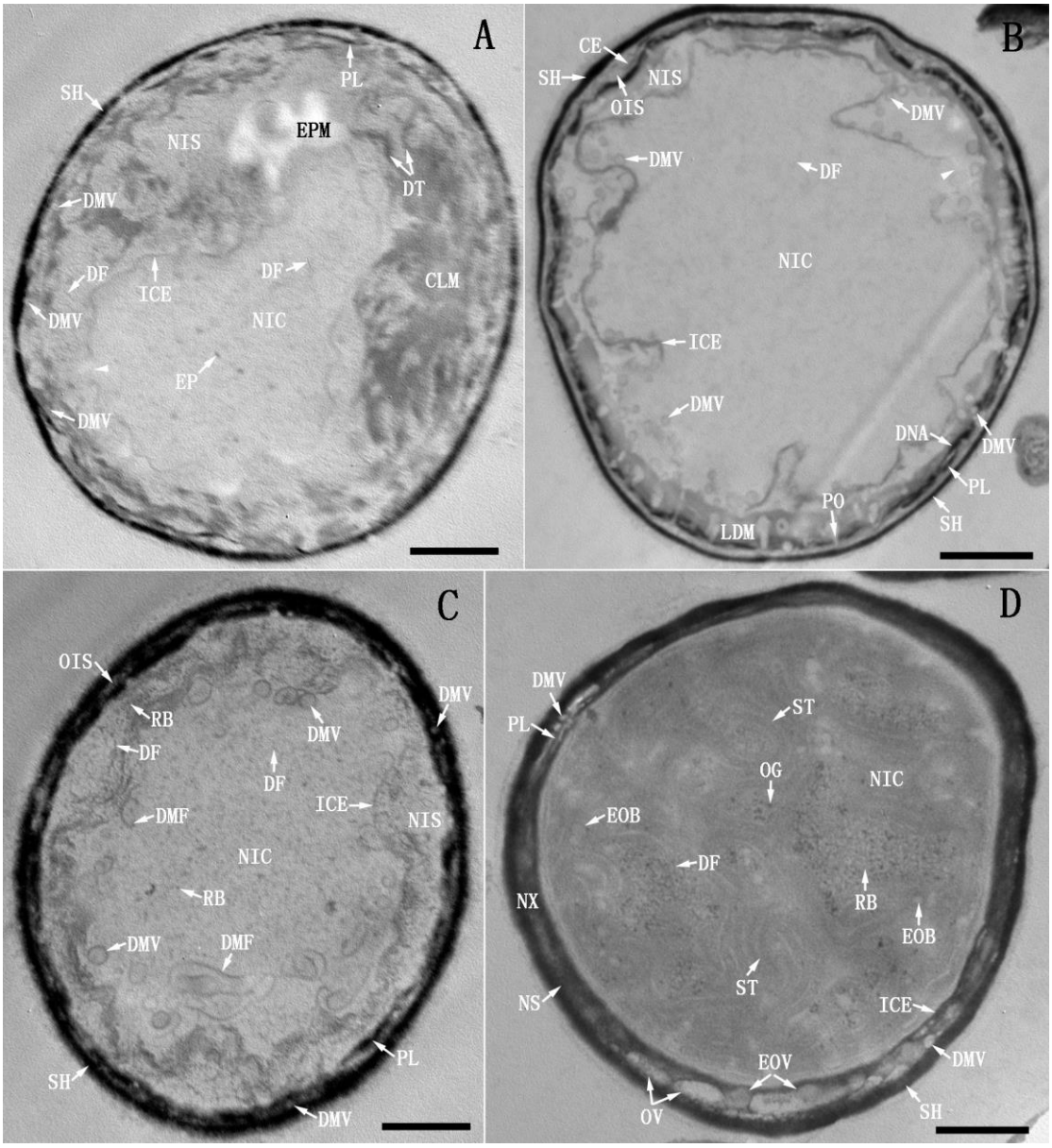

Figure 6. Re-compartmentalization, reallocation of DNA and formation of secondary thylakoids. (**A**) As DMS extended into a double-membraned intracytoplasmic envelope (ICE), a new inner cytoplasm (NIC) and a new inner intracytoplasmic space (NIS) were re-compartmentalized. Most of the DNA fibers were relocated in NIS, which decondensed into cloudlike materials (CLM) or aggregated into DNA threads (DT). By contrast only few DF and electron-dense particles (EP) were partitioned into NIC. ICE was not sealed, so substances could be exchanged through its opening (arrowhead). Interestingly, some electron-transparent materials (EPM) were synthesized on the outer leaflet of ICE. (**B**) Accompanying the expansion of ICE, DMV in NIS moved into NIC via ICE opening (arrowhead), or passed through PL pores (PO) into OIS. (**C**) After ICE sealed, DNA in NIS recondensed into a mass of DF with concomitant formation of countless RB. Meanwhile, an increased number of DF emerged and some RB were formed in NIC; DMV began to open up and re-transformed into DMF and elongated. (**D**) DMF in NIC extended into PCB-less secondary thylakoids (ST) with concomitant formation of OG and electron-opaque bodies (EOB) as well as enrichment of DF and RB. Outside of NIC, the major portion of PL was dismantled, such that NIS and OIS coalesced into a new intracytoplasmic space (NS), whose confluent content became the new intracytoplasmic matrix (NX). Aside from DMV, electron-translucent oblong vesicles (OV) and electron-opaque vesicles (EOV) emerged in NS. Scale bar, 0.5 μm.

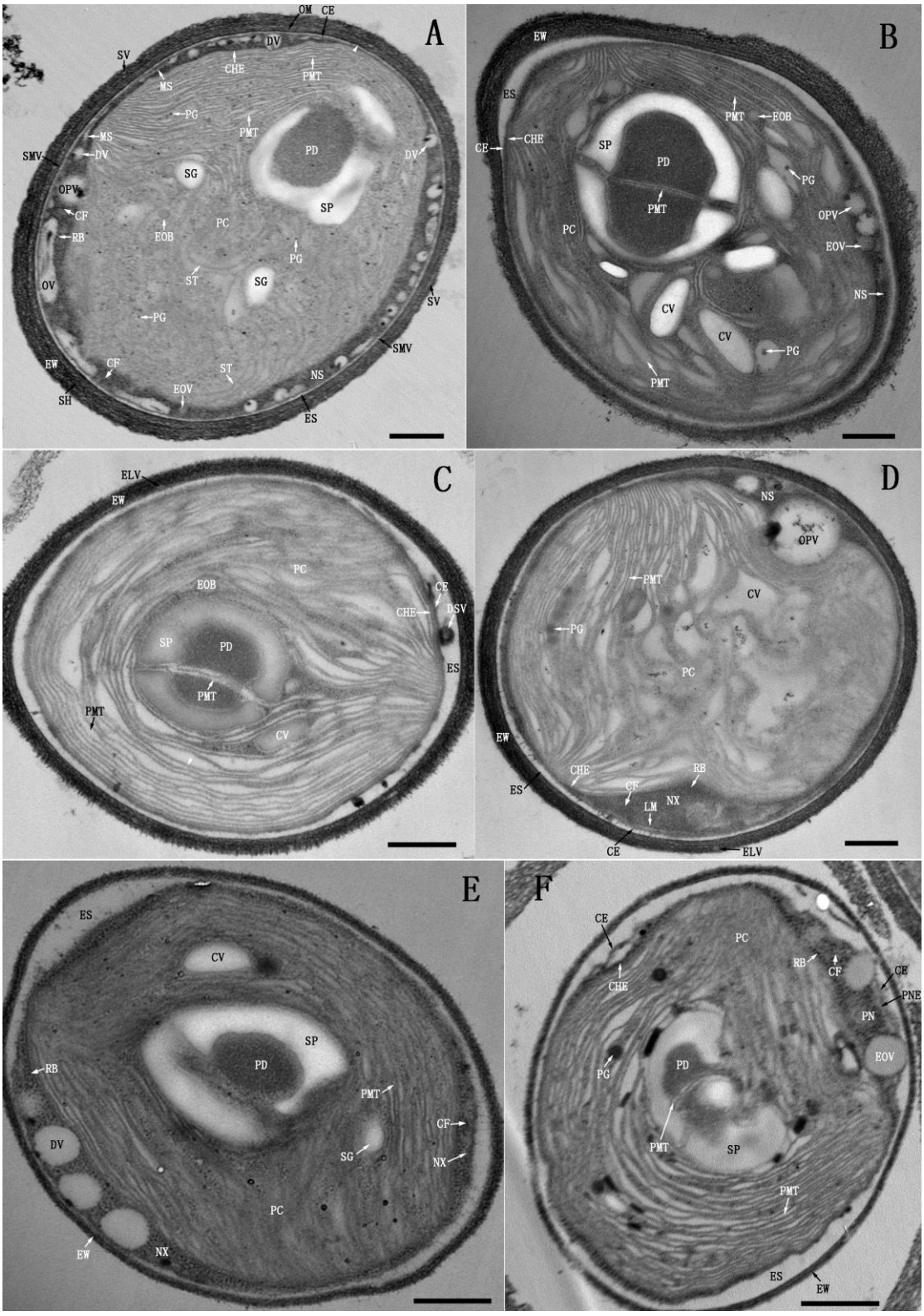

Figure7. Biogenesis of primitive chloroplast, eukaryotic cell wall and primitive nucleus. (**A**) ST was disassembled leaving some remnants in the lower region of the polarized NIC, while parallel arrays of primitive eukaryotic thylakoids (PMT) were being developed from the plastoglobuli (PG) in upper region of NIC with concomitant formation of a nascent pyrenoid (PD) surrounding by an incomplete starch plate (SP), and two starch granules (SG). So, NIC developed into the primitive chloroplast (PC), and ICE became the chloroplast envelope

(CHE). Inside NS, thick chromatin fibers (CF) and large RB were formed; PL and DMV disappeared; while many small dotted vesicles (DV) and opaque-periphery vesicle (OPV) emerged. Some DV began to fuse and flattened into membrane segments (MS). Outside of NS, some smaller vesicles (SMV) shed from the outer leaflet of CE into ES; while the peptidoglycan layer (P) of CW turned into an electron-dense layer (EL) (arrowhead), and a stratified SH embedded with small vesicles (SV) was formed external to OM, hence the compacted CW and SH became the eukaryotic cell wall (EW). (**B**) PMT with wide luminal space were formed continuously by elongation of CV; PD got matured with a complete SP, bisecting by two pairs of PMT. The expanded PC occupied most of NS in longitudinally sectioned plane. (**C**) PC filling with PMT occupied whole NS, such that NS disappeared in longitudinally sectioned plane, CHE adhered to CE, from which a dense vesicle (DSV) shed off into the widened ES. (**D**) A vertical section of cell. The anterior PC portion occupied the surrounding NS, so EX was pushed to the shrinking NS around the posterior portion of PC, at the border of which MS fused into a limiting membrane (LM). (**E**) An oblique section through the posterior half of cell, in which most of the NX aggregated at one side of PC. (**F**) A tangential section through the posterior end of cell. All NX converged at one side of PC, which was encased by LM and thus turned into the primitive nucleus (PN) containing CF, RB and EOV; while LM became the primitive nuclear envelope (PNE). NS vanished and in turn CE shrank and wrapped PC and PN. Scale bar, 0.5 μm.

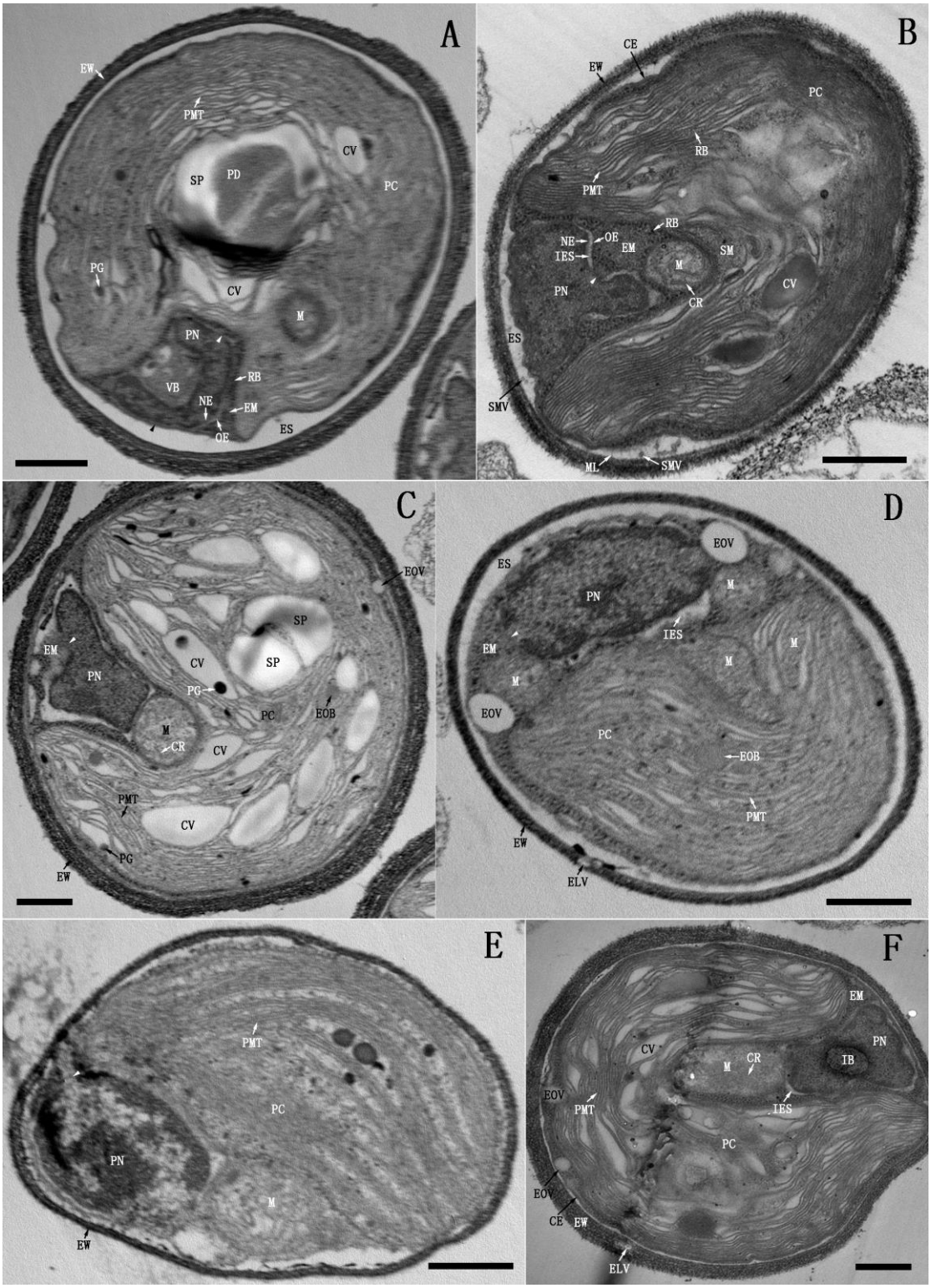

Figure 8. Concurrent formation of eukaryotic cytoplasm and biogenesis of mitochondria. (**A**) PN was engulfing a vesicle-containing body (VB) with concomitant extrusion of nuclear matrix, i.e. the eukaryotic cytoplasm (EM). PNE comprised a nuclear envelope (NE) and an outer nuclear envelope (OE), which was contiguous with CE at the outer side (black arrowhead), but separated in PC cavity. EM was extruded from PN at the site where NE and OE fused (white arrowhead), and concurrently a mitochondrion (M) was assembled in PC. (**B**) PC with enriched stroma (SM) further invaginated, in the apical dome of its cavity, a mitochondrion with

characteristic cristae (CR) emerged. OE and NE of the enlarged PN were separated by an inter envelope space (IES), but came into contact a one site and fused into a large opening (arrowhead), from which the nuclear matrix (i.e. EM) was expelled. In the meantime, a number of SMV and microfibrils (ML) budded and emanated from CE into ES. (**C**) PN expelled EM from the fused opening of NE and OE (arrowhead) in the presence of a newly formed spherical mitochondrion. (**D**) A large PN extruded EM (arrowhead) in the presence of two mitochondria, while two spindle-shaped mitochondria were being assembled within PC. (**E**) PN expelled EM (arrowhead) coincident with the appearance of a spindle-shaped mitochondrion. (**F**) A large PN contained a membrane-delimited intranuclear body (IB). Scale bar, 0.5 μm.

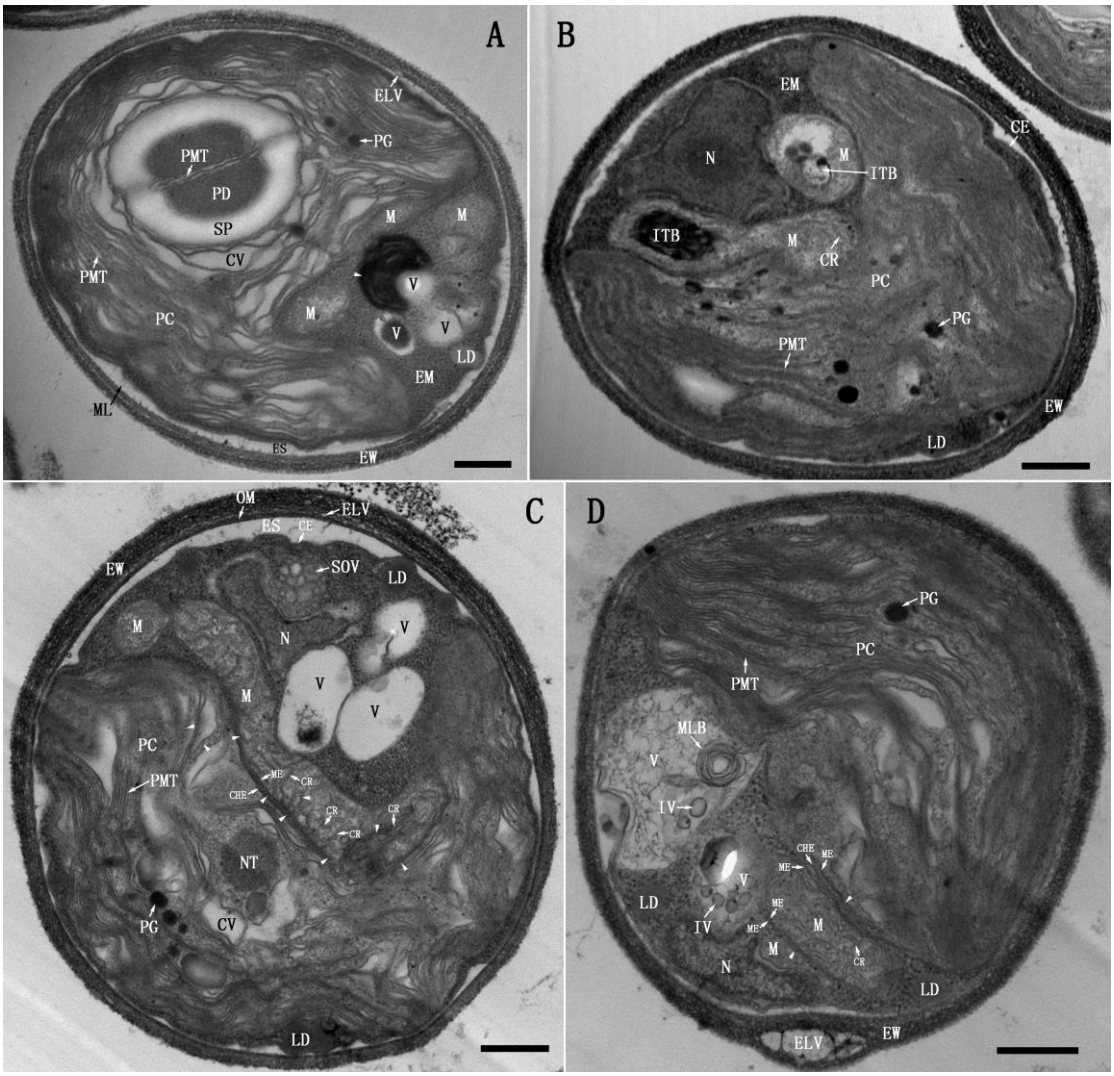

Figure 9. Biogenesis of mitochondria after building up EM. (**A)** After formation of EM, PN got matured into nucleus (N); while a small mitochondrion was being developed in PC in the presence of two mitochondria, three vacuoles (V), a lipid droplet (LD) and some electron-dense materials (arrowhead). (**B**) A twisting dumbbell-shaped mitochondrion was nearly finished, one of its bulbous-end containing an internal body (ITB) was segregated, but the other was contiguous with PC. Another mitochondrion within EM also sequestered an ITB. (**C**) A large 'L-shaped' mitochondrion was being assembled in the presence of three vacuoles and a cluster of small opaque vesicles (SOV), which was continuous with PC in the region around its corner point. The inner side mitochondrial envelope (ME) and the corresponding portion of CHE as well as CR were all synthesized by fusion of the dense-margined vesicles (DGV) (arrowhead) that were developed by segmentation of PMT. There was a large nucleoid-like structure (NT) in the venter side of PC. (**D**) After emergence of the large vacuoles with internal vesicle (IV) and multilamellar body (MLB), a bulky mitochondrion was being developed, which was connected with PC on the inner side but a small mitochondrion on the outer side. In the inner and outer interfaces, three and two pairs of contorted membranes were being synthesized respectively by merging DGV (arrowhead). In addition, several large ELV were embedded in EW. Scale bar, 0.5 μm.

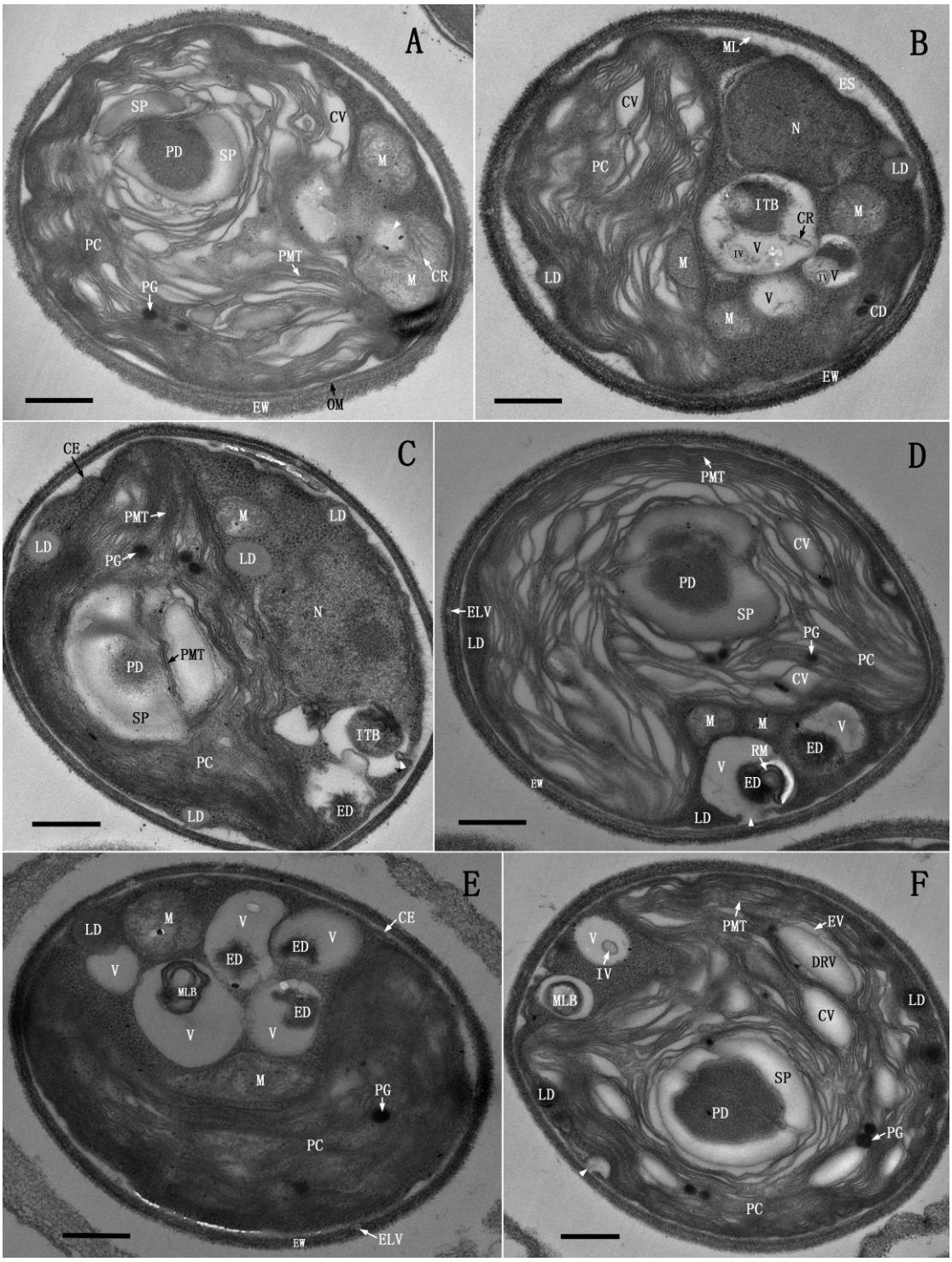

Figure 10. Biogenesis of vacuoles (**A**) The matrix of a mitochondrion was being degraded (arrowhead). (**B**) After matrix degradation, the mitochondrion turned into a vacuole containing ITB, IV and remnant CR or only electron-transparent matrix. Meanwhile, a new mitochondrion was being developed in PC, a LD was formed at CE and a piece of chloroplast debris (CD) emerged in EM. (**C**) ITB in two small mitochondria degraded into electron-dense debris (ED); while ITB in the large vacuole remained intact, the vacuolar membrane fused with CE and invaginated (arrowhead) (**D**) a small vacuole expelled ED into EM; while a large vacuole sequestered some residual membranes (RM), the membranes of which contacted and fused with CE, resulting in an opening

(arrowhead). (**E**) A large vacuole contained MLB, while a small vacuole extruded a LD into EM. (**F**) Two vacuoles contained MLB and IV respectively. A small vacuole fused with CE, giving rise to an opening (arrowhead); and several cobblestone-shaped DRV emerged in EV. Scale bar, 0.5 μm.

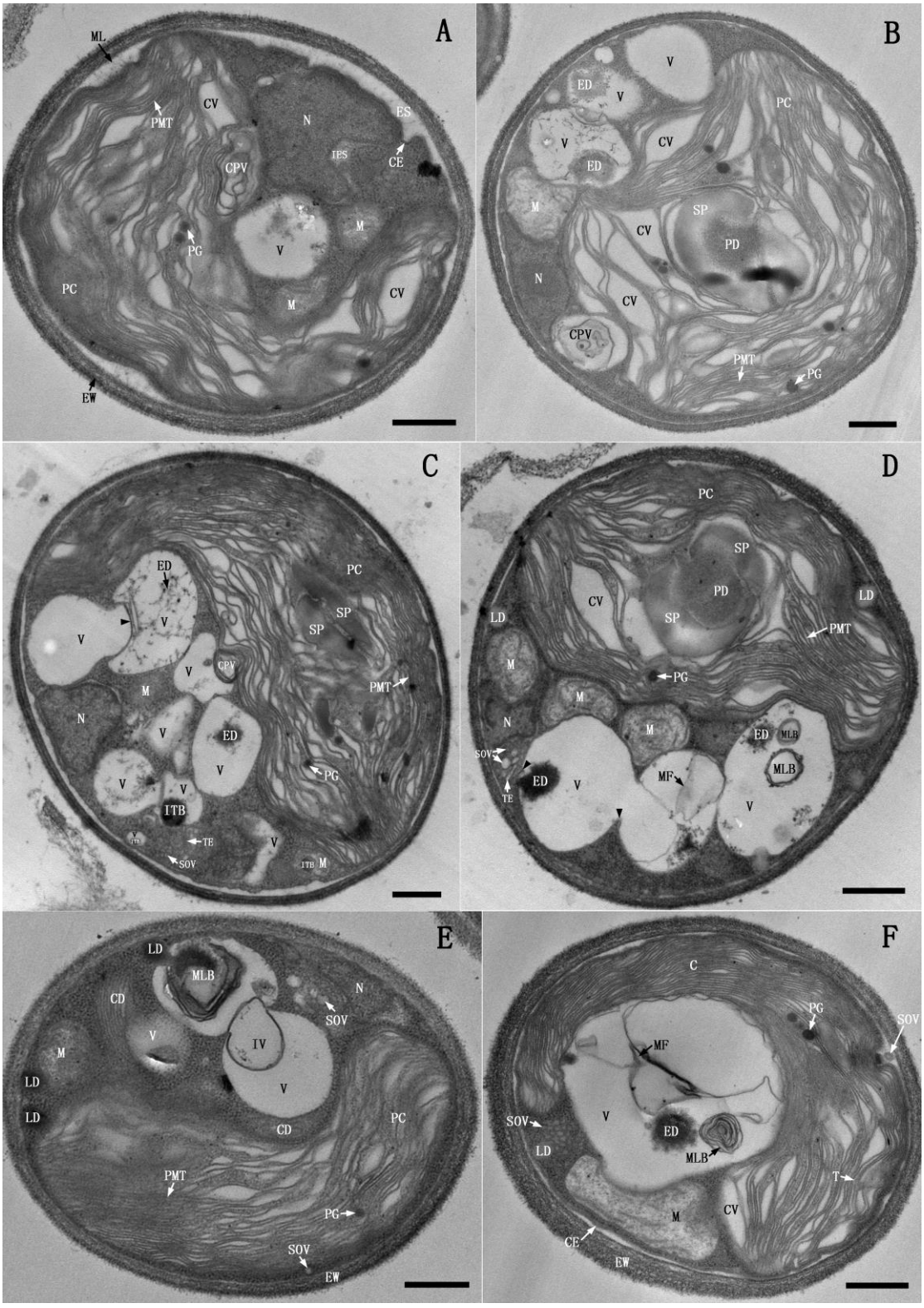

Figure 11. Formation and degradation of PMT-derived vesicles and coalescence of vacuoles. (**A**) A collection of short PMT 'rolled up' into "vesicle within vesicle" like compound vesicle (CPV) in PC margin. (**B**) A CPV was segregating from PC into EM. (**C**) A CPV was detaching from PC into a vacuole; while a large vacuole protruded into another one (arrowhead). (**D**) Membranes of the protruded vacuoles and the vacuole that contained membranous fragments (MF) fused at their contact site (arrowhead). (**E**) Two vacuoles were merging, in which a

LD was extruded from MLB; while a conspicuous piece of CD presented in EM. (**F**) PC got matured in chloroplast (C); all vacuoles coalesced into a single vacuole containing ED, MF and MLB. Scale bar, 0.5 μm.

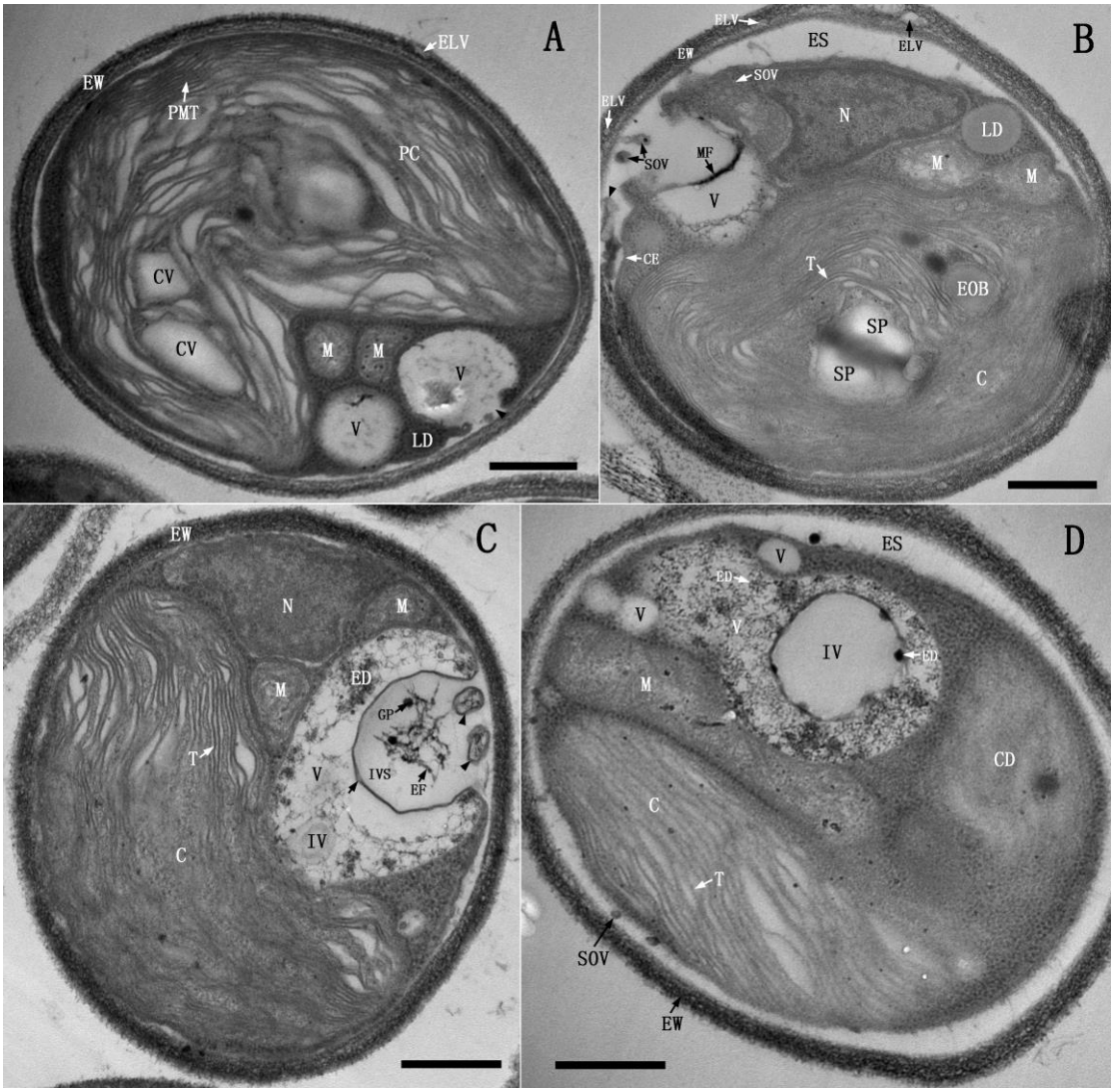

Figure 12. Vacuole mediated unconventional exocytosis and endocytosis. (**A)** An opening was formed at the contact site of the vacuolar membranes and CE (arrowhead), from which the vacuolar content was released. (**B**) The contacted vacuolar membranes and CE broke up into fragments (arrowhead)，resulting in a wide opening, from which the soluble contents and SOV were expelled outside into ES. (**C**) The vacuolar membranes merged with the CE at two distant sites and then invaginated, resulting in a large invaginated space (IVS) entrapping some electron-dense fibrils (FB) and globular particles (GP); while CE between the two merged sites disrupted and coiled into membranous structures (arrowhead). It was clear that the invaginated vacuolar membranes consisted of two unit membranes (arrow). (**D**) A vacuole contained a large IV, which was in contact with a sausage-shaped mitochondrion and close to a CD. Scale bar, 0.5 μm.

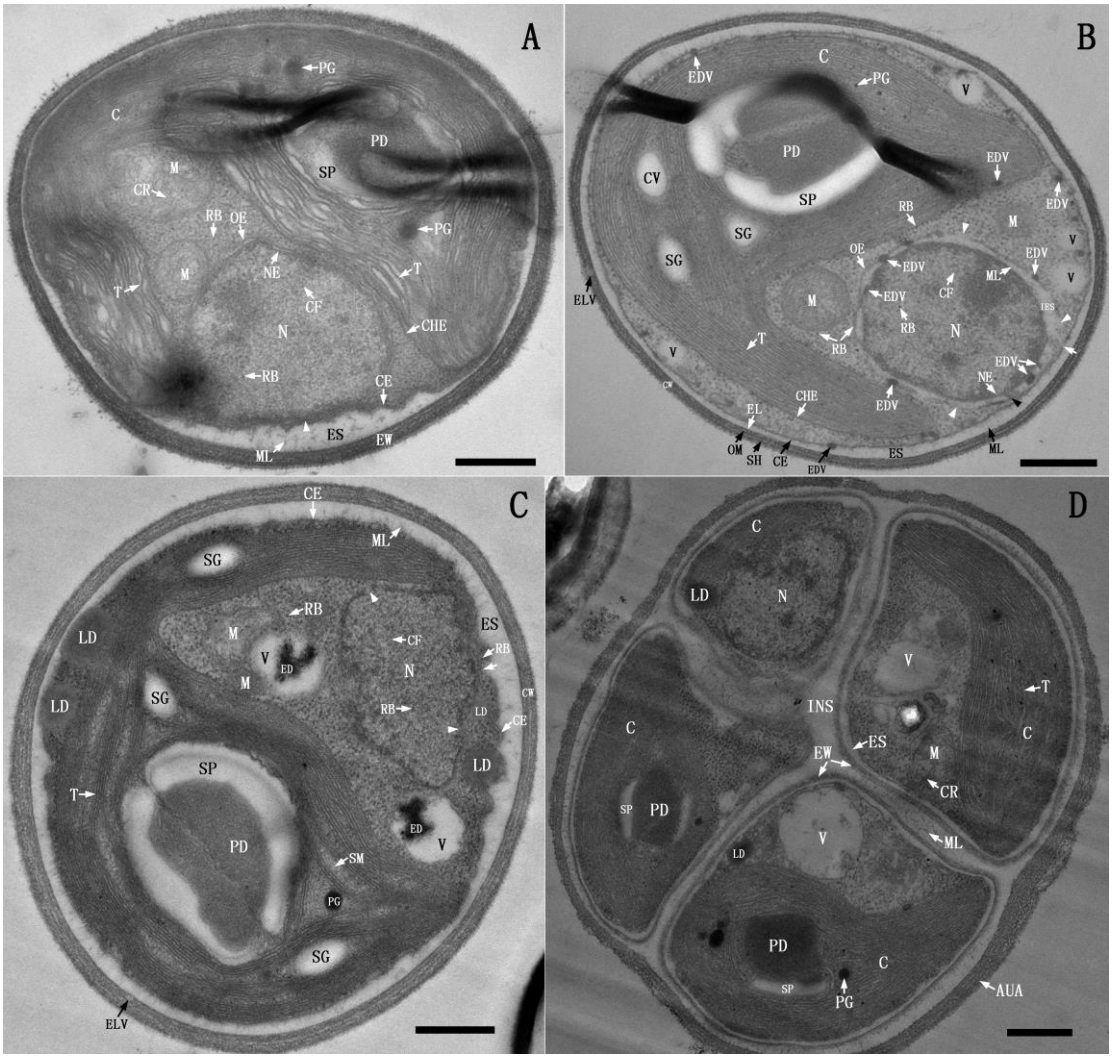

Figure 13. Structure and reproduction of TDX16-derived eukaryotic cell. (**A**) A TDX16-derived eukaryotic cell (TDX16-DE cell) contained an 'e'-shaped chloroplast (C), a nucleus (N) and two mitochondria. The nucleus contained CF and some RB, whose OE and NE contacted and appressed to CE at the opening of chloroplast cavity (arrowhead). (**B**) Electron-dense vesicles (EDV) budded form NE (black arrowhead) into IES, and then fused with and re-budded from OE, ultimately reached the inner side of CHE and the two sides of CE. There were several openings at OE (white arrowhead), and one opening at the contact site of OE and CE (arrow). (**C**) OE and NE contacted intimately, on which large openings (arrowhead) were formed, and amazingly a fusion pore or conduit was formed at the contact site of NE, OE and CE (arrow). (**D**) Four developing autospores in an autosporangium (AUA) were segregated from each other by the wide interspace (INS). Scale bar, 0.5 μm.

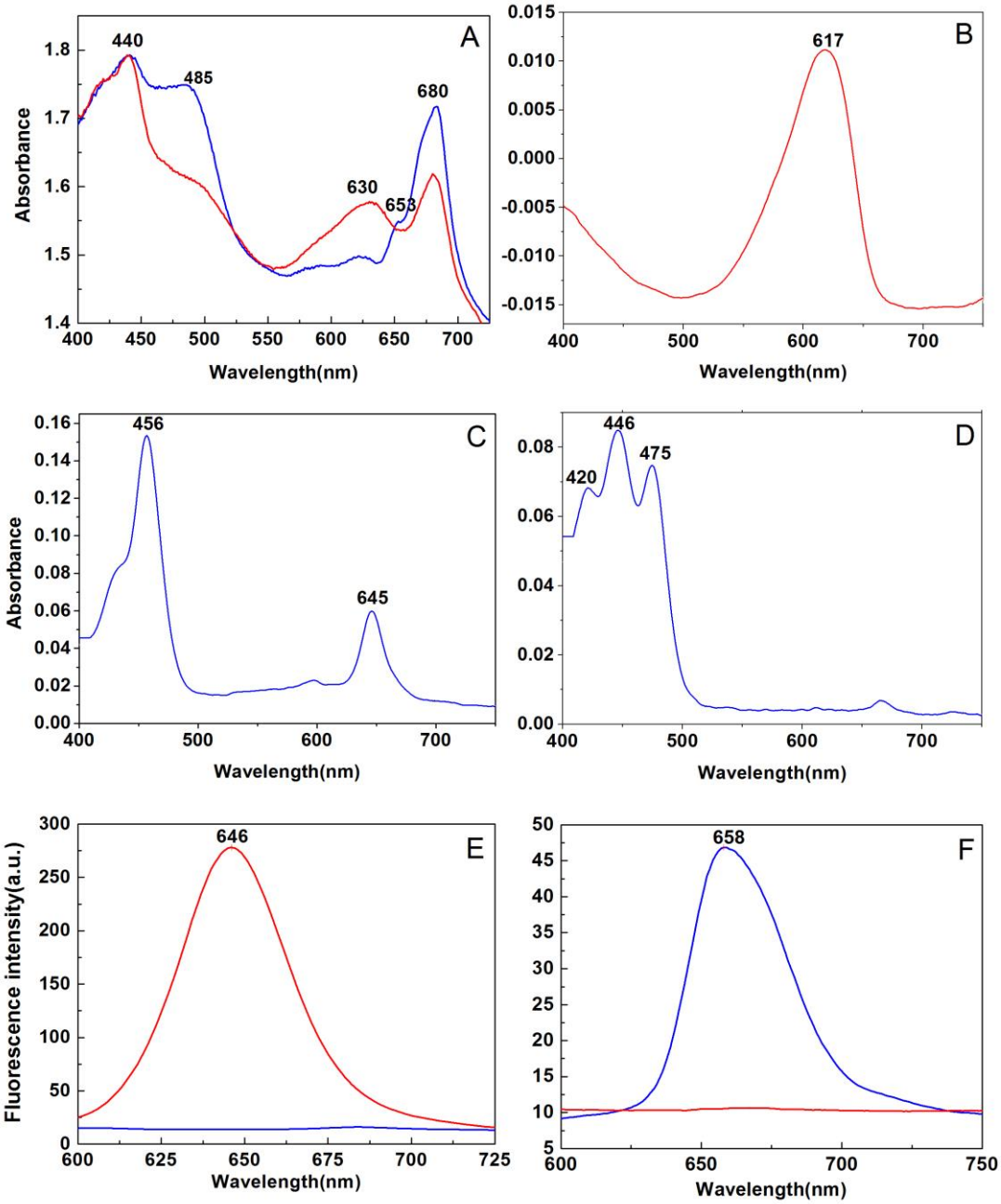

Figure 14. Absorption and fluorescence emission spectra. (**A**) In vivo absorption spectra of TDX16 (red) and TDX16-DE cell (blue). Absorption spectra of phycocyanin (PC) (**B**), chlorophyll b (**C**) and lutein (**D**). Fluorescence emission spectra of water soluble pigment extracts (**E**) and lipid soluble pigment extracts (**F**) of TDX16 (red) and TDX16-DE cell (blue).